Title
Curing and Subsurface Damage Monitoring of Epoxy and Epoxy-based Composites

Author
Fan, Gaochen

Publication Date
2017

UNIVERSITY OF CALIFORNIA, SAN DIEGO

Curing and Subsurface Damage Monitoring of Epoxy and Epoxy-based Composites

A thesis submitted in partial satisfaction of the
requirements for the degree Master of Science

in

Materials Science and Engineering

by

Gaochen Fan

Committee in charge:

Professor Kenneth J. Loh, Chair
Professor Michael T. Tolley
Professor Sheng Xu

2017

The Thesis of Gaochen Fan is approved, and it is acceptable in quality and form for publication on microfilm and electronically:

Chair

University of California, San Diego

2017

DEDICATION

To Mom, Dad, and Grandma

TABLE OF CONTENTS

LIST OF FIGURES

ACKNOWLEDGEMENTS

I would first like to thank my thesis advisor, Dr. Kenneth J. Loh, for his support and guidance. Anytime when I was struggling with problem related with research or life, he always patiently guided me and provided suggestions that encouraged me to move forward. His guidance helped me learn how to be a researcher, and I am grateful to have him as my advisor and mentor.

Secondly, I would like to acknowledge and express my sincere gratitude to my lab colleague and friend Mr. Sumit Gupta. Since I first joined the lab, he helped and taught me various aspects of research, ranging from conducting scientific experiments to technical writings. I cannot imagine how difficult it would be without his support and help. For this thesis, the ECT code used was developed by him, and some materials included in the thesis are works we accomplished together.

Parts of Chapter 2 and the entirety of Chapters 3, 4, and 5 are reprints of the material as it appears in Noncontact Epoxy Curing Monitoring and Subsurface Damage Detection, Proceedings of the 11th international workshop on structural health monitoring, 2017, Gupta S, Fan G, Loh KJ, and Noninvasive Monitoring of Epoxy Curing. IEEE Sensors Letters, 2017, 1(5), Gupta S, Fan G, Loh KJ.. The thesis author was the primary investigator and co-author on these two papers. In addition, some of the work that appears in this thesis was submitted for consideration for publication in Curing and Subsurface Damage Monitoring of Epoxy-based Composites, Structural Health Monitoring, 2017, Fan G, Gupta S, Loh KJ. The thesis author was the primary investigator and first author of this paper.

Finally, I would like to thank my mom, dad, and grandma. They have always been my strongest supporters, and their love and support are the reason for my accomplishments today.

VITA

2015	B.S.	Purdue University, West Lafayette, USA
2017	M.S.	University of California, San Diego, USA

PUBLICATIONS

1. Gupta S, **Fan G**, Loh KJ. Noncontact Epoxy Curing Monitoring and Subsurface Damage Detection 11th international workshop on structural health monitoring; Stanford, CA: Destech Publications, Inc; 2017.
2. Gupta S, **Fan G**, Loh KJ. Noninvasive Monitoring of Epoxy Curing. IEEE Sensors Letters. 2017;1(5).
3. **Fan G**, Gupta S, Loh KJ. Curing and Subsurface Damage Monitoring of Epoxy-based Composites. Structural Health Monitoring. 2017. Submitted for pulication.

ABSTRACT OF THE THESIS

Curing and Subsurface Damage Monitoring of Epoxy and Epoxy-based Composites

by

Gaochen Fan

Master of Science in Materials Science and Engineering

University of California, San Diego, 2017

Professor Kenneth J. Loh, Chair

Due to their extraordinary material properties, epoxy has been widely used in various industries. Moreover, nanomaterials are infused into epoxy to enhance their mechanical performance and for encoding different functionalities, such as for fiber reinforced polymer (FRP) composites. However, additives in the epoxy matrix can affect curing and the mechanical properties of FRP structures. Therefore, the main objective of this thesis was to investigate the use of electrical capacitance tomography (ECT) for monitoring curing and subsurface damage in pristine epoxy and nanocomposite epoxy. In short, ECT uses a set of noncontact electrodes and interrogates a sensing area using different patterns of electric field excitations. Boundary capacitance measurements obtained simultaneously are used as inputs for solving the ECT inverse problem to reconstruct the electrical permittivity distribution of the sensing area. The hypothesis was that curing and damage of epoxy would result in permittivity changes that could be detected and localized by ECT. The thesis first starts with a detailed description of the ECT theory and system. Second, to test the hypothesis, pristine epoxy was subjected to ECT for monitoring curing, which was then validated using ultrasonic wave tests. Then, ECT was used to monitor the curing of carbon nanotube-based epoxies whose electrical properties are sensitive to strain. Both pristine and nanocomposite epoxy results confirmed the hypothesis that permittivity decreased with increasing curing time, and ECT can be used as a noncontact and noninvasive curing monitoring tool. Last, epoxy specimens with different geometries were drilled with holes to simulate damage. The results indicated that ECT was not only able to reconstruct the shape of the specimens but was also able to identify the location and severity of damage.

Chapter 1. Introduction

1.1. Background of fiber reinforced polymer (FRP) composites

For more than six decades, fiber reinforced polymer (FRP) composites have been widely used for various engineering applications. In short, multiple layers of carbon fiber, graphite, and glass fiber fabrics are stacked and infused with epoxy to facilitate load transfer and to realize the FRP part [1]. Their superior mechanical properties with a high strength-to-weight ratio and excellent corrosion resistance have made them attractive for aerospace, automotive, biomedical, and various other industries [2, 3]. Despite their advantages, FRPs and epoxy-based composites are susceptible to different damage modes. For instance, incomplete epoxy curing can cause tremendous reduction in mechanical properties, including the strength, stiffness, and fatigue life of FRPs. Most of the damage in FPRs occurs internally, which is very difficult for technicians to detect. Thus, the main objective of this thesis was to develop a noncontact and portable technique for technicians to perform rapid assessment of the state of curing of epoxy, as well as to detect the presence of subsurface defects (or damage).

The technology of FRP reinforcement started to gain momentum in the 1980s in order to eliminate the long, difficult, and high-cost construction cycle. Moreover, it can be applied to complex structures which are difficult to reinforce and, at the same time, keep the structure in the original size [4]. In the aerospace industry, billions of dollars have been spent on research and development to make FRP composites suitable for manufacturing lightweight subsonic and supersonic aircrafts while replacing the secondary structures in civilian aircrafts [3]. For example, the Airbus A310 uses carbon composites as a replacement for the aluminum (Al) alloy using in the vertical stabilizer, resulting in 400 kg of weight saving. The use of FRP composites was further extended to the horizontal stabilizer and secondary control surface for the A320, saving a total of 800 kg in weight as compared to the conventional Al alloy unit. It should be mentioned that, with 1 kg of weight reduction, 2,900 L of fuel can be saved each year. More recently, the Boeing 787 is made of over 50 *wt.*% (80 *vol.*%) of composites materials, which are used extensively in the fuselage, wings, tail, doors, and interior. Since the 1980s, Bell Helicopters (Dallas Fort Worth, Texas) have been applying composite technology to their airframe, leading to 20% of weight reduction, and all their new vehicle blades are built from composites [5].

Due to their broad use and high demand, there is an urgent need to understand and prevent failure of FRP composites. FRP composites are notch-sensitive materials, and their structural integrity can be significantly affected when damage occurs [6]. Many studies have investigated improving the properties and functionalities of FRP composites to prevent sudden damage and to extend service life. Coope *et al.* [7] developed Diels-Alder based self-healing epoxies for FRP composites. To achieve self-healing, the composites were heated at 150 ºC for 5 min, and fracture load was measured as an indication of healing efficiency. The highest healing efficiencies were 122% for the bulk material and 123% for thin films with three repeated healing cycles. Fire-resistant polymeric nanocomposites were studied and developed by George *et al.* [8], where atmospheric pressure plasma treatment was conducted to increase surface energy. A polybenzimidazole (PBI) coating was applied on phenolic composite that resulted in an increase in thermal stability from 280 ºC to 350 ºC. Calcium silicate nanopowders were also incorporated in the PBI-coated composites, which exhibited a thermal stability of 380 ºC for 2.5 *wt.*% and 420 ºC for 7.5 *wt.*%. However, the lack of *in situ* damage detection techniques have always been an issue, especially once these FRP composites are implemented in practice. The damage of FRP either initiates during the manufacturing process (*e.g.*, improper curing) or during the service life (*e.g.*, impact damage) [6]. Thus, it is necessary to develop a technique for monitoring FRP composites during manufacturing, as well as to detect damage when the structure or component is service. A review of these topics is presented in sections 1.3 and 1.4.

1.2. Epoxy background

Since the discovery of epoxy resins in 1909 [9], they have been one of the most widely used materials in various industries due to their extraordinary mechanical properties, high adhesiveness to different materials, and good heat and chemical resistance. Their excellent cohesive and adhesive properties, which provide the abilities to bind and transfer load to the fibers in FRP composites, make epoxy one of the most broadly used matrix materials for FRPs [1]. Epoxy resins are thermosetting polymers formed by 3D crosslinking of low molecular weight epoxide monomers during curing. They are being used as adhesives [10], coatings [11], encapsulating materials [12] and in FRP composites [13]. In addition, they are finding new uses in healthcare for wound dressing, vascular grafting, and artificial aortic heart valves [14], especially since epoxy resins can be formed to shape complex and fine geometries due to their low viscosity prior to curing.

There are many types of epoxy, to name of few, bisphenol-A epoxy resins, cycloaliphatic epoxy resin (CAE), trifunctional epoxy resins, tetrafunctional epoxy resins and novolac epoxy resins. This research is focus on a type of bisphenol-A epoxy resins, diglycidyl ether of bisphenol-A (DGEBA), which is produced by epichlorohydrin reacting with bisphenol-A. The molecular weight of the DGEBA, which represents the number of repeat units, has great effect on its properties. The higher molecular weight, the more viscous the resin will be [15, 16].

The curing reaction of epoxy resin can occur when reacting with different curing agents under a variety of curing conditions. Some of the curing reactions are controlled or accelerated by the curing agent. The curing reaction is irreversible, and the molecular structure of the curing agents will result in different cure kinetics and glass transition temperatures of the epoxy. According to chemical compositions, the curing agents can be categorized as amine-type, alkali, anhydrides, and catalytic curing agents. Various curing conditions can also be employed, such as room-temperature curing, heat curing, and photo-curing. In this study, an aliphatic amidoamine curing agent was used to react with the epoxy resin at different temperatures [17, 18]. The experimental details will be discussed in greater depths in later chapters of this thesis.

1.3. Current state-of-art of damage detection

In addition, manufacturing defects (*e.g.,* subsurface voids and cracks) can form in the epoxy matrix, which can propagate to cause severe or even catastrophic failure if they remain undetected [19]. Thus, the ability to detect subsurface damage at an early stage is critical for ensuring the safety, reliability, and remaining load-carrying capacity of epoxies. To date, visual inspection is the most frequently used method to detect damage in structures. However, manufacturing defects and subsurface damage that develop during service may not be visible and remain undetected. Moreover, visual inspection is time-, labor-, and cost-intensive.

To overcome this limitation, pre-embedded sensors such as strain gages and optical fibers can be employed for strain monitoring and damage detection. These sensors are embedded at pre-selected points of the structure to detect the microscopic changes in length or defamations [20]. Electrical strain gages are widely used for structure health monitoring, since electrical strain sensing is a well-developed technology which can produce proper results with relatively low cost equipment and sensors [20]. However, electrical strain gages are less capable in damage detection for composites applications, because they are limited to surface strain measurement, require wire connections, and degradation may occur during long term fatigue conditions [20]. Therefore, optical fiber sensors especially wavelength based fiber Bragg grating (FBG) sensors become popular in composites SHM applications. FBG sensors can be directly embedded into the composite material due to the small size, and can offer long term stability under harsh environments [21, 22]. Nevertheless, FBG sensors are still point sensors where measurements can only be obtained at discrete points where the sensors are attached. A dense network of sensors is often required for accurate performance evaluation and structural health monitoring.

Acoustic emission (AE) monitoring is a damage detection technique that has been used for FRP composite structures (*e.g.,* wind turbine blades). The AE phenomenon can be explained by the transient release of elastic energy that occurs during crack imitation and propagation, matrix delamination, debonding, breaking of fibers, and other deformations [23]. Piezoelectric sensors are employed and attached to the structural surface to detect the elastic waves generated by the deformations or damage processes that occur within the material. Dutton *et al.* [24] demonstrated the capability of AE monitoring for identifying the location of the damage and failure area, as well as estimating the severity of damage based on the amplitude and energy of AE signals. However, AE monitoring is difficult to apply to FRP structures during service due to the high level of background noise [20].

Thermal imaging method is a nondestructive subsurface defect detection technique that evaluates the temperature difference on the target surface by using infrared cameras or sensors. Electromagnetic radiation emitted by the structure is measured, and a temperature-thermal image is reconstructed using the emitted energy [25]. Thermoelastic stress method is one of the specific thermal imaging technique that is based on the effect where the temperature of elastic solids change as applied stress changes [26]. Hai-Ali *et al.* [27] applied thermoelastic stress methods to orthotropic composite materials for determining the stress distribution of isotropic materials. The drawback of thermal imaging is that it can only penetrate a few millimeters in depth of the structure. Furthermore, environmental conditions (*e.g.*, cloud cover, solar radiation, and wind speed) can significantly influence infrared thermography tests and the corresponding results [25].

Ultrasonic and guided-waves are well-established techniques and widely used for investigating the inner structure and integrity of composite materials. In short, guided-waves or Lamb waves (generated by piezoelectric transducers) propagate through the structure of interest. Once the wave encounters a defect, it scatters. Then, these signals will be captured by sensors, which can then be compared with the same sensor measurements of the undamaged structure. Therefore, defects or damage can be identified and located [28]. Ultrasonic C-scan is another popular noninvasive technique for identifying voids, porosity, inclusions, resin starvation, and delamination in FRP composites. The spatial location of misalignments in fiber orientation in FRPs can also be identified by scanning the surface using ultrasonic waves generated by the piezoelectric transducer during C-scanning. The drawbacks of ultrasonic techniques are their limitation to small-scale applications, and they are not accurate for complex structures. For Ultrasonic C-scan , the specimen needs to be immersed in water (as a coupling agent) [3, 29].

Modal-based methods are most commonly used today for damage detection [30]. In general, the modal parameters (*e.g.*, natural frequencies, mode shapes, and damping, to name a few) are obtained from structural vibration measurements that can be generated by ambient means or forced excitations. These modal parameters can be regarded as functions of the physical properties of the structure, and any changes captured in the modal tests can be utilized to detect and locate damage [31]. The most significant limitation of modal-based damage detection methods is that small and localized damage cannot be easily resolved using modal-based methods [32]. Furthermore, they require accurate measurements of modal frequencies and mode shapes, and it is sometimes difficult to obtain these measurements accurately due to sensor noise and inherent error of the models.

1.4. The current state-of-art of epoxy curing monitoring

As mentioned earlier, the covalent bonds formed during curing govern the properties of thermosetting epoxy resins, while improper curing can adversely impact mechanical properties. It is necessary to precisely and timely monitor the curing process of epoxy to obtain the best performance of the product. To prevent incomplete curing or premature demolding, manufacturers tend to apply an exceeding amount of curing time due to the lack of an *in situ* curing monitoring technique. However, the long cure time can also cause over-curing of epoxy, leading to reduction in material properties. Currently, thermal techniques (*e.g.*, differential scanning calorimetry (DSC), differential thermal analysis (DTA), and dynamic mechanical analysis (DMA), to name a few) are widely used for monitoring epoxy curing, where information about their degree, rate, and completion of curing can be obtained [33-35]. Although these techniques can provide detailed and precise curing kinetic analysis of epoxy to develop more efficient manufacturing curing processes, they are not suitable for *in situ* curing monitoring applications.

Shigue *et al.* [35] showed that dielectric thermal analysis (DETA) can utilize the dielectric response of epoxy as a precursor for monitoring curing. Here, a parallel-plate capacitor setup was used with epoxy resin as the dielectric medium, and impedance and temperature were measured as the epoxy cured. Hardis *et al*. [33] proposed the use of Raman spectroscopy and dielectric analysis (DEA) for evaluating the curing state of fiber-reinforced epoxy and compared the results to DSC tests. Glass fiber grafted with multi-walled carbon nanotubes (MWCNT) has been incorporated into epoxy for curing monitoring purposes by Tzounis *et al*. [36]. The resistance was measured during 24 h of curing cycle, and a significant increase in resistance was observed, which could be used to indicate the curing stage of epoxy. However, many of these methods cannot be performed *in situ*, often require ideal laboratory conditions, and are not suitable for large-scale applications. Therefore, better monitoring strategies are still needed for understanding and optimizing curing.

1.5. Multifunctional epoxy-based composites

Besides using pristine epoxy as the matrix material to create multifunctional FRP structures (*e.g.*, with the added capability of sensing damage), a significant body of work has focused on incorporating conductive additives (*e.g.*, colloidal silica, carbon black (CB), graphene, and carbon nanotubes (CNT), to name a few) in epoxy resin during manufacturing [37, 38]. Among these, CNTs are popular due to their intrinsic superior mechanical properties and high electrical conductivity. A CNT-epoxy composite, which can be employed as an electrical heating element and stable temperature sensor, was developed by Neitzert *et al.* [39]. At a low concentration of CNTs (*e.g.*, 0.5 *wt.*%), the resistivity of the composites decreased monotonically as temperature increased, which was explained by a fluctuation-induced tunneling conduction model. The interrelation between mechanical properties and interfacial molecular structure in CNT-epoxy composites was studied by Lachman *et al.* [40]. The interfacial stress-transfer efficiency could be improved by attaching different functional groups to the nanotube surface. The effects of curing temperature, mixing rate, weight fraction, and size of CNTs on the strain sensitivity of CNT-infused epoxy composites were systematically studied by Hu *et al.* [41]. Even though incorporating nano-fillers in epoxy can enhance their material properties and multi-functionality, these additives could adversely affect curing.

1.6. Research objective and thesis outline

The objective of this thesis was to investigate a new sensing modality based on electrical capacitance tomography (ECT) for monitoring epoxy curing and subsurface defects, particularly in pristine and strain-sensitive nanocomposite epoxies. The proposed method works by interrogating a region of space with different patterns of electric field excitations and simultaneously measure the capacitance response at the boundary electrodes; a ECT system setup is shown in Figure 1.1. The capacitance measurements were then used as inputs for solving the ECT inverse problem of reconstructing the electrical permittivity distribution of the interrogated sensing region. It was hypothesized that the dielectric property (*i.e.,* permittivity) of epoxy changes during curing or if damage (*e.g.,* voids) is present in the material. This thesis begins with a description of the background and theoretical formulation of ECT (*i.e.,* forward and inverse problems) in

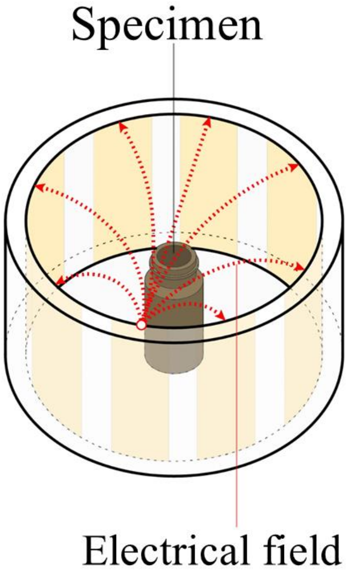

Figure 1.1. A simplified 3-D schematic of ECT system is shown.

chapter 2. Chapter 3 focuses on demonstrating ECT as a technique for monitoring curing of pristine epoxy, and the results were validated by comparing them to ultrasonic mechanical property characterization results. Then, in chapter 4, the fabrication of CNT-infused epoxy is presented, and the CNT-infused epoxy was subjected to electromechanical testing, curing, and ultrasonic tests. A comparison between pristine and CNT-infused epoxy was also conducted, and the results are presented in this chapter. The demonstration of subsurface damage detection using ECT is presented in chapter 5 for different shapes and damage sizes. Finally, chapter 6 ends with a conclusion and discussion of future research directions.

Chapter 2. ECT Background

2.1. Introduction

ECT is a soft field imaging technique that aims to reconstruct the electrical permittivity distribution of a predefined region. This is achieved by propagating an alternating current (AC) electric field through a circular sensing region, while all other remaining electrodes remain grounded, as is depicted in Figure 2.1 [42]. Then, the capacitance between the excitation and grounded electrode pairs are measured. This measured set of capacitances are used to solve an inverse problem to reconstruct the corresponding permittivity distribution of the sensing region.

Since its discovery in the late 1980s, ECT has been successfully used for different flow monitoring applications [43-46]. It has also been used for monitoring other industrial processes (*e.g.,* visualization of flame during combustion [47] and nylon-polymerization reaction monitoring [48], to name a few). Others have shown the potential of ECT as a nondestructive evaluation (NDE) tool [49-51]. More recently, Gupta *et al.* [52] has successfully validated ECT for monitoring the curing process of pristine epoxy resins. In this thesis, it was hypothesized that the permittivity values of epoxy and nanocomposite epoxy changes as they cured and become damaged, which can be detected by ECT. Similar to other tomographic techniques, ECT contains the forward problem and inverse problem. First, the forward problem of ECT seeks to solve the boundary capacitance response based on a known permittivity distribution and electrical field excitation. Second, the ECT inverse problem uses an iterative Gauss-Newton algorithm to estimate the permittivity distribution based on measured boundary capacitance response due to an applied electric

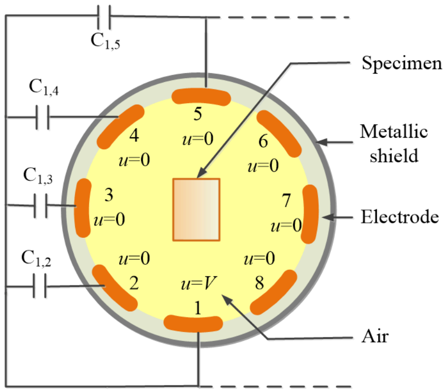

Figure 2.1. The schematic of the eight-electrode ECT system is shown.

filed excitation. The mathematical formulation of the ECT forward and inverse problems are discussed in greater depths in the next sections that follow.

2.2. Forward problem

The ECT forward problem seeks to estimate the mutual capacitances between excitation and sensing electrodes, where the electrical permittivity distribution (ε) of the sensing region (Ω) (*i.e.*, bounded by the electrode array) is known *a priori*. The ECT forward problem is defined by the 2D Laplace's equation, and assuming steady state condition in the region of interest:

$$\nabla \cdot (\varepsilon \nabla u) = 0 \tag{2-1}$$

where u is the electrical potential distribution in Ω. The finite element method (FEM) is applied to solve this second-order partial differential equation with proper boundary conditions to evaluate the field distribution in Ω. The signal applied is an AC square wave voltage signal. The magnitude used was 15 V peak-to-peak with a frequency of 1.25 MHz. A set of linear equations (2-2) will be obtained from the FEM results:

$$Ku = I \tag{2-2}$$

where K represents the stiffness matrix of the system calculated from equation (2-1), and I is the force vector that is obtained from the boundary conditions. Once u is evaluated, equation (2-3) is used to estimate the mutual capacitance between the excitation and sensing electrodes by:

$$C_{i,j} = \frac{1}{V}\int_{e_j} \varepsilon \frac{\partial u_i}{\partial n} dl \quad i = 1:L;\ j = i+1:L \tag{2-3}$$

where n is the unit inward normal to the j^{th} measurement electrode, e_j is the length of that same electrode, V is the magnitude of applied voltage, L is the total number of electrodes in the electrode array, and u_i is the solution of the forward problem when the i^{th} electrode is used for excitation.

2.1. Inverse problem

While the ECT forward problem is employed to estimate the mutual capacitances between boundary electrodes, for practical applications, an inverse problem needs to be solved to reconstruct the permittivity distribution using experimental measurements of boundary capacitance responses developed due to the given applied electric field excitation. The objective of the inverse problem is to minimize the norm of the error vector between the experimental measured capacitances (C_m) and computed capacitances (C_c) to a threshold value of 0.05% used in this work, while permittivity distribution is updated during each iteration of the optimization scheme.

The inverse problem is a nonlinear and ill-posed problem by nature, where large changes in permittivity distribution can result in minute changes in boundary capacitance responses. Hence, a Gauss-Newton iterative algorithm was developed and implemented for spatial permittivity reconstruction. The algorithm started with an initial assumption of permittivity distribution, and the forward problem was solved to obtain its corresponding C_c. This was followed by calculating the error vector (e) based on the difference between C_m and C_c, as shown in equation (2-4):

$$e = C_m - C_c \tag{2-4}$$

C_c could be represented using $F(\varepsilon)$, which is the forward problem operator that can obtain the capacitance values at the boundary electrodes based on a given spatial permittivity distribution (ε). Total variation regularization was applied by adding a penalty term in the minimized cost function (p) as shown in equation (2-5):

$$p = \arg\min[\|F(\varepsilon) - C_m\|^2 + \alpha^2 \|R(\varepsilon - \varepsilon_0)\|^2] \tag{2-5}$$

where α is the regularization parameter, R is the regularization matrix, and ε_0 is the assumed background permittivity distribution. By using linear approximation around the solution ε_i for the i^{th} iteration step, the permittivity for ε_{i+1} could be estimated. In order to obtain the minimum value, the first derivative of $F(\varepsilon_i)$ was computed and set to zero, and the permittivity distribution difference ($\Delta\varepsilon_i$) could be estimated by taking the derivative. Then, $\Delta\varepsilon_i$ was added to the permittivity value ε_i, followed by repeating and solving the forward problem using the updated permittivity distribution to predict the corresponding boundary capacitance response, C_c and the new error vector (e).

Next, the error ratio (ζ) was estimated, which is defined as the ratio between the norm of the error vector and the norm of measured boundary capacitance. The error ratio was checked to see if it is smaller than or equal to the specified threshold value of 0.05% used in this thesis.

$$\xi = \frac{\|e\|^2}{\|C_m\|^2} \leq 0.05\% \tag{2-6}$$

Thereafter, permittivity distribution was updated, and the process repeats for as long as the condition specified in equation (2-6) was not satisfied. Once the ζ reaches or falls below the threshold value, iteration stops and the resulting permittivity distribution was assumed to closely represent the true permittivity distribution of the sensing region. In this thesis, the initial assumption was that the sensing domain was uniformly filled with air with a uniform permittivity distribution of 8.85×10^{-12} F/m. This assumption not only closely resembled actual testing conditions, but it also helped reduce the total number of iterations required to satisfy the error threshold [53, 54].

2.4. Summary

In summary, ECT seeks to reconstruct the electrical permittivity distribution using capacitance measurements obtained at the boundary of a sensing region. Here, the sensing region is defined as the 2D area enclosed by an array of equidistantly spaced electrodes arranged in a circular fashion. Experimentally, an electrode was selected and excited with an AC signal while the others electrodes were grounded. The mutual capacitance between the excitation and grounded electrodes were simultaneously measured. This procedure was repeated but with a different excitation electrode. Then, an inverse problem, using the set of measured capacitances as inputs, could be solved to reconstruct the spatial permittivity map. The inverse problem computed the difference between the experimental capacitance measurements and forward problem capacitance calculations. When the difference is larger than the predefined error threshold, the algorithm iterated and updated the permittivity distribution. The ECT inverse problem iterated until the error threshold criterion is satisfied, before then outputting the reconstructed permittivity map.

Chapter 3. Pristine Epoxy Curing Monitoring

3.1. Introduction

As mentioned in chapter 1, epoxy is one of the most widely used materials in FRP composites and many other industries. However, accurate *in situ* monitoring of epoxy curing has always remained challenging. The covalent bonds formed during curing govern the properties of thermosetting epoxy resins, while improper curing can adversely impact mechanical properties. For example, impregnated air voids reduce the elastic and shear strengths of fiber-reinforced polymer composites and compromises structural integrity and performance [55]. Thus, the ability to monitor curing *in situ* is crucial for maintaining manufacturing quality, structural performance, and in some cases safety or liability. Most epoxy curing monitoring techniques (*e.g.*, differential scanning calorimetry [56], fluorescence method [57], and Raman Spectroscopy [58], to name a few) help gain insights about the polymeric reactions occurring during curing. However, these methods are time consuming and are constrained to smaller specimen sizes.

The primary objective of this chapter is to develop and validate a noncontact, noninvasive system that could rapidly assess the state of epoxy curing. It was hypothesized that the electrical permittivity of epoxy resins changes as they cure over time, which could be monitored by ECT. First, in this chapter, quick-curing epoxy was used to validate the capability of ECT to capture the curing-induced permittivity changes over time. Second, ECT was used to map the permittivity distribution of aerospace-grade epoxy specimens as they cured from 0 to 24 h. Also, specimens at different curing times were also compared using ECT. Last, the mechanical properties (*e.g.*, storage modulus and Young’s modulus) of specimens (at different curing stages) were determined using ultrasonic testing to validate the ECT results.

3.2. Validation of ECT for epoxy monitoring

3.2.1. Experimental procedure

A set of ECT validation tests were performed using pristine quick-curing epoxy. The objective of these validation tests was to demonstrate that ECT can be used to monitor curing in quick-curing epoxy (*i.e.*, 5 min of set time and 30 min of handling time). Preparation of the epoxy specimens begun by thoroughly mixing the resin and hardener, at a 1:1 ratio, by hand for 1 min. For validating curing monitoring, the resin and hardener mix were pour into 20 mL glass vials. Each specimen was immediately placed in the center of the ECT sensing region, and a set of ECT measurements were obtained to capture the specimen's initial electrical permittivity. Each specimen cured in ambient room temperature, while ECT measurements were recorded every 5 min until 35 min of complete curing.

3.2.2. Validation results

As mentioned earlier, ECT was employed for monitoring the change in electrical permittivity of epoxy as it cured and transformed from a viscous fluid state to that of a solid state. The reconstructed permittivity distributions of a representative epoxy specimen during 35 min of curing are shown in Figure 3.1. First, it can be observed from all the ECT results that the circular specimen was successfully identified in the middle of the sensing domain. Second, the permittivity of the specimen decreased dramatically over the course of 35 min as the viscous epoxy mix cured to become solid. To better quantify the change in electrical permittivity over time, the maximum relative permittivity from each ECT

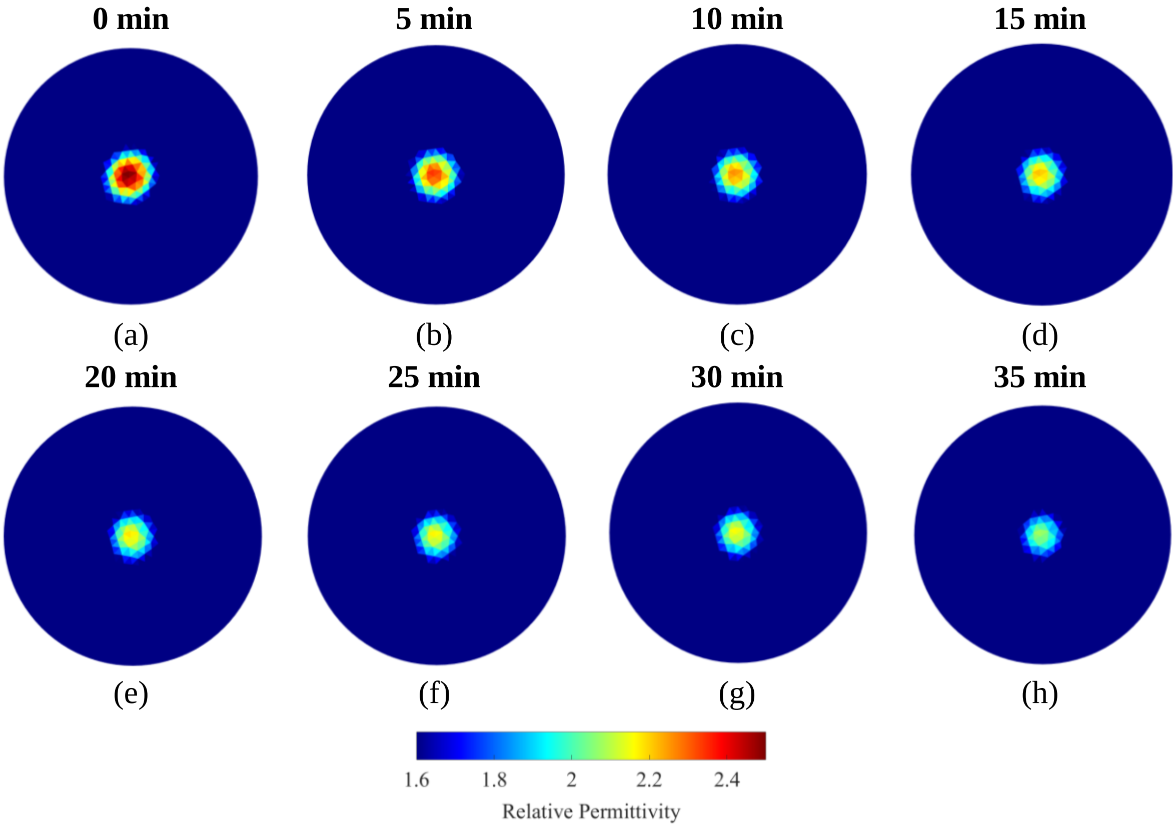

Figure 3.1. The ECT results of an epoxy specimen after curing for (a) 0, (b) 5, (c) 10, (d) 15, (e) 20, (f) 25, (g) 30, and (h) 35 min are shown.

image was extracted and plotted as a function of time in Figure 3.2. Figure 3.2 clearly shows that the epoxy specimen's electrical permittivity decreases from ~ 2.47 to ~ 2.13 and in an exponential manner. Overall, the results demonstrated that ECT could successfully capture the gradual change in electrical permittivity as pristine epoxy cured.

3.3. Experiment details

3.3.1. Specimen preparation

Upon validating the use of ECT for assessing epoxy curing in quick-curing epoxy, the remainder of this thesis focused on aerospace-grade epoxy specimens. In this section, a two-part epoxy (using EPON Resin 825 and Epikure Curing Agent 3046, which were provided by Hexion Inc.) was used for ECT curing monitoring experiments and ultrasonic mechanical characterization. The epoxy resin and curing agent were first subjected to high-speed shear-mixing at 2,000 rpm for 10 min with a 2:1 mass ratio (*i.e.*, resin to curing agent). Then, the mixture was transferred into 20 mL glass vials to cast specimens for curing monitoring tests or into 20 mm-diameter plastic tubes for ultrasonic mechanical property tests. Curing of all epoxy specimens was performed in ambient room temperature.

3.3.2. ECT curing monitoring tests

ECT was employed for noninvasive monitoring of epoxy curing. First, the ECT interrogation-DAQ (or data acquisition) system consisted of eight boundary electrodes equidistantly spaced to form a 120 mm-diameter circular sensing region. When one electrode was used for excitation, the DAQ system recorded capacitances at all other electrodes, giving 8×7/2=28 unique capacitance measurements. Second, five identical EPON 825 epoxy specimens were prepared and tested using ECT. Each specimen was placed in the center of sensing region as shown in Figure 3.3a and interrogated to obtain

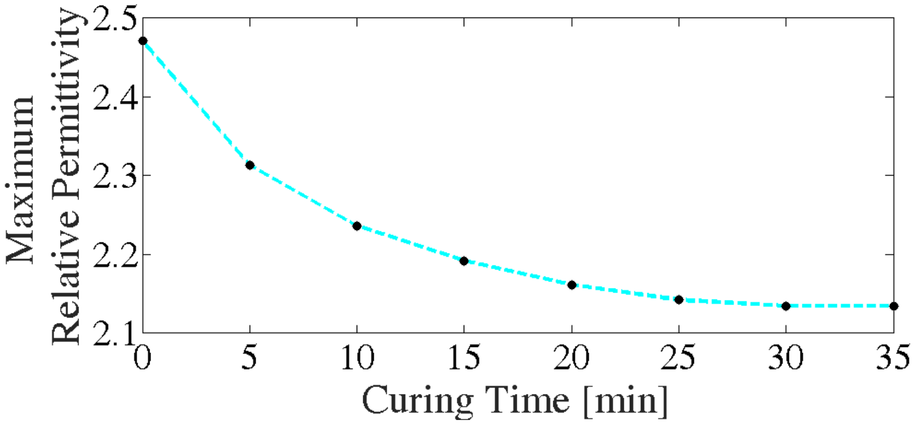

Figure 3.2. The maximum relative permittivity of quick-curing epoxy specimen with respect to curing time from 0 to 35 min are shown.

the corresponding set of boundary capacitance data. Starting from 0 h of curing, ECT tests were performed every 1 h until the specimen fully cured after 24 h.

The next test was to show that ECT could simultaneously differentiate between specimens undergoing different stages of curing. First, two epoxy specimens, which were cured for 13 h and 14 h, were placed in two locations in the electrode array and subjected to ECT measurement and data acquisition to compare the permittivity differences as shown in Figure 3.3b. Similarly, as Figure 3.3c indicated, three specimens that were cured for 13, 14, and 24 h were also simultaneously interrogated. For all the tests, capacitance data acquired by ECT were used as inputs to the ECT inverse problem for reconstructing the permittivity distribution maps.

3.3.3. Characterization of epoxy mechanical properties

The mechanical properties of epoxy specimens during curing were characterized *in situ* using ultrasonic testing [59] to further validate the ECT monitoring results. Ultrasonic wave propagation is widely accepted for characterizing the mechanical properties of

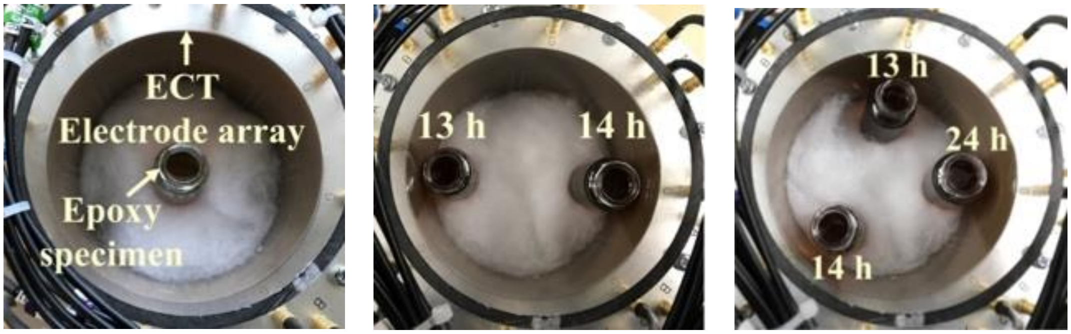

(a) (b) (c)

Figure 3.3. (a) An epoxy specimen is placed in the electrode array for ECT interrogation and data acquisition. (b) Two epoxy specimens subjected to 13 h and 14 h of curing were also simultaneously interrogated, (c) followed by testing three specimens cured for 13, 14, and 24 h.

.

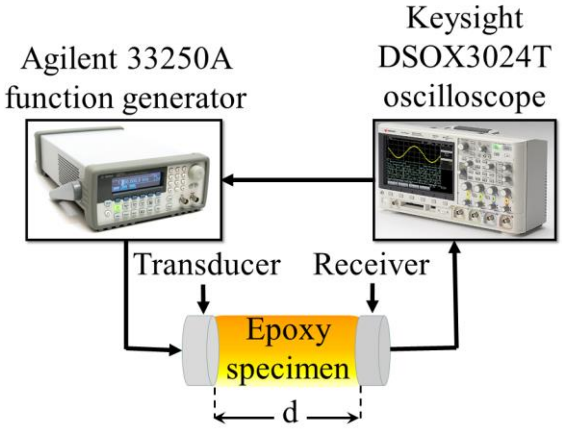

Figure 3.4. The schematic illustrates ultrasonic wave test setup for monitoring the change in mechanical properties of epoxy specimens throughout curing.

materials. According to Maffezzoli *et al*. [59], ultrasonic waves could be used as a source of dynamic mechanical deformation in order to obtain the longitudinal storage modulus. The storage modulus, which represents the viscoelastic properties of uncured epoxy, and Young’s modulus, which describes the stiffness of its solid phase, were measured by propagating ultrasonic longitudinal and shear waves, respectively, using a pitch-catch setup [60]. The test setup entailed mounting lead zirconate titanate (PZT) transducers at opposite ends of the epoxy specimen. An Agilent 33250A function generator excited one PZT using a 1 MHz pulse waveform, and the response was recorded by measuring the generated voltage response of the PZT mounted at the opposite end, using a Keysight DSOX3024T oscilloscope, as shown in Figure 3.4. Two types of PZT were used in this series of tests, where longitudinal wave PZT was employed to obtain velocity and attenuation data for storage modulus calculations, and shear wave PZT was used to obtain p-wave and s-wave velocity to calculate Poisson’s ratio and Young’s modulus. Testing began after specimens were cured for 15 h, because this was the minimum curing time for which the mixture

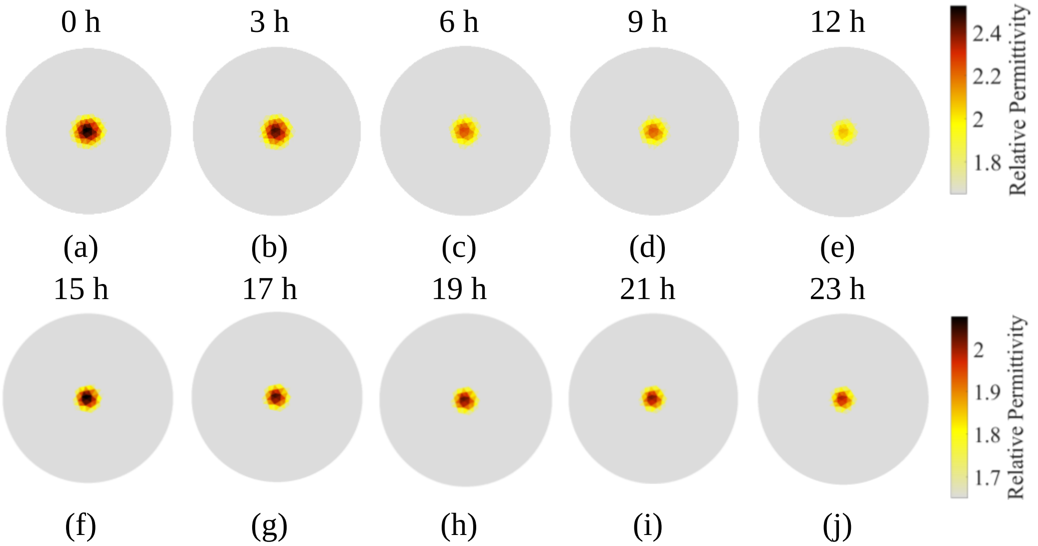

Figure 3.5. Relative permittivity distributions of epoxy specimens subjected to different curing times were reconstructed using ECT. ECT results of an epoxy specimen cured for (a) 0, (b) 3, (c) 6, (d) 9, and (e) 12 h are shown. The same specimens were further cured for 24 h and the corresponding reconstructed permittivity distributions for (f) 15, (g) 17, (h) 19, (i) 21, and (j) 23 h are shown.

transitioned from a viscous liquid to a glassy transition state where a reliable shear wave peak could be detected using the PZT receiver. Thereafter, ultrasonic tests were conducted every 1 h until 24 h of complete curing. Three specimens were prepared and tested for obtaining representative storage modulus and Young’s modulus of the epoxies at different stages of curing.

3.4. Results and discussion

3.4.1. Noninvasive epoxy curing monitoring

As previously stated, ECT was used for monitoring epoxy curing. Figure 3.5 shows relative permittivity distributions acquired at different stages of curing as an epoxy specimen was cured for 24 h. First, ECT successfully identified that the specimen was located in the center of the sensing domain. Second, Figure 3.5 shows that uncured epoxy showed higher relative permittivity in its initial stages, particularly when it was still a

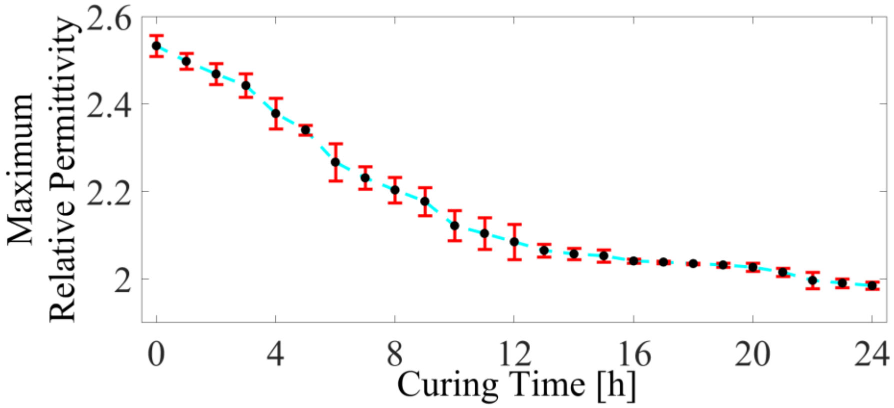

Figure 3.6. The ECT results were processed for five different epoxy specimens, and the average of maximum relative permittivity of all specimens are plotted with respect to total curing time. The error bars correspond to the standard deviations.

viscous liquid. As curing progressed with epoxy transitioning to become solid, relative permittivity decreased, which can be explained by the decrease of ion mobility as epoxy cured and solidified.

Figure 3.6 plots the maximum relative permittivity (*i.e.*, average of five specimens' ECT results) with respect to curing time, and the error bars are the standard deviations. The maximum relative permittivity value decreased from ~2.54 to ~1.98, and this result is consistent with the quick-curing epoxy result. Figure 3.6 follows an exponential decay, where the rate of change of relative permittivity is higher at earlier stages but slows down with increasing curing time before reaching a plateau. This trend is consistent with the slowdown of curing over time as fewer free epoxy functional groups remain in the mix to react.

The sensitivity of the ECT system was also verified by testing two and three specimens simultaneously (Figure 3.3), where each specimen was cured to different stages.

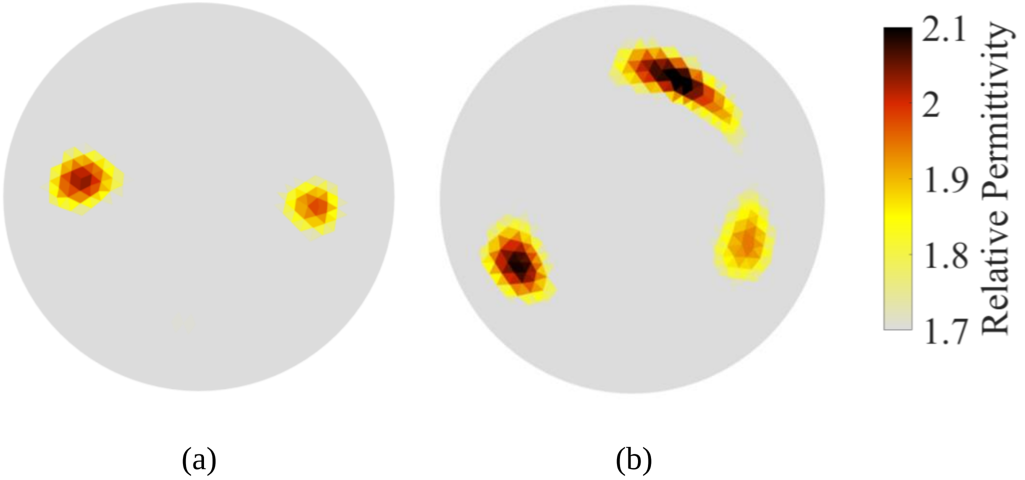

Figure 3.7. The relative permittivity maps for (a) two specimens subjected to 13 and 14 h of curing and (b) three epoxy specimens cured for three different durations (*i.e.*, 13, 14, and 24 h) are shown.

Figure 3.7a suggests that the relative permittivity of the 13 h specimen on the left is higher than the 14 h one on the right, which is consistent with previous results. Similar results were also obtained when three specimens were tested simultaneously, and Figure 3.7b confirms that ECT can not only monitor dielectric property changes with high accuracy but can also accurately pinpoint where these electrical permittivity changes are occurring in the sensing domain. However, some of the errors (*e.g.*, elongated permittivity changes of the 24 h-cured specimen in Figure 3.7b) were likely due to measurement noise in the experimental measured boundary capacitances. It should be noted that noise, as well as the number of electrodes, regularization scheme, FEM mesh, and sensing domain to specimen size ratio, all contribute to the overall sensing resolution of ECT.

3.4.2. Mechanical properties of epoxy

To further validate ECT, the storage and Young's moduli of epoxy specimens during curing was characterized by ultrasonic tests. First, to determine storage modulus, the longitudinal wave velocity (V_L) and attenuation coefficient (α) were computed. V_L can be expressed using time-of-flight (t) and specimen thickness (d):

$$V_L = \frac{d}{t} \tag{3-1}$$

where d was 25 mm, and t was the time difference between the start of the excitation pulse and the arrival of the first peak signal received. Here, α is related to the decrease in amplitude between successive peaks, which can be calculated using:

$$\alpha = \frac{1}{3d} 20 \log\left(\frac{A_0}{A}\right) \tag{3-2}$$

where A_0 is the amplitude of the peak excitation signal, and A is the second peak's amplitude detected by the PZT receiver as shown in Figure 3.8. For the pitch-catch setup

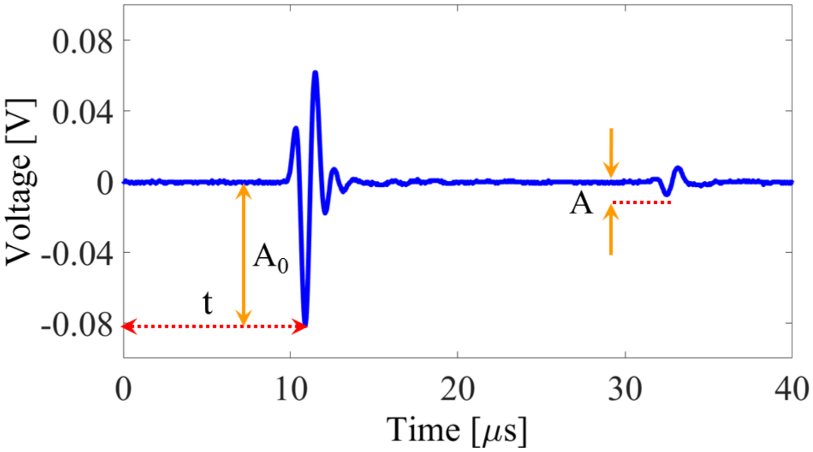

Figure 3.8. Ultrasonic pitch-catch tests were performed to estimate the storage modulus of the epoxy specimens. The amplitude of incident and reflected wave is identified in the plot.

used, the distance travelled by the ultrasonic wave was equivalent to three times the specimen thickness (*d*) as shown in Figure 3.4. Then, storage modulus (*E'*) was found using:

$$E' = \frac{\rho V_L^2\left[1-\left(\frac{\alpha(V_L/\omega)}{2\pi}\right)^2\right]}{\left[1+\left(\frac{\alpha(V_L/\omega)}{2\pi}\right)^2\right]} \quad (3\text{-}3)$$

where ρ is epoxy density (calculated to be 1,130 g/cm^3), ω is signal frequency (1 MHz), and V_L/ω is wavelength.

Second, Young's modulus was calculated by measuring p-wave velocity (*i.e.*, pressure wave, V_p), s-wave velocity (*i.e.*, shear wave, V_s), and Poisson's ratio (ν). Even though a shear wave transducer was used, a weak p-wave was still generated and was the first signal peak received; the second and major peak observed was the s-wave. Time-of-flight of the two waves were measured to compute V_p and V_s. With these quantities, Poisson's ratio was calculated by:

$$v = \frac{V_P^2 - 2V_S^2}{2(V_P^2 - V_S^2)} \quad (3\text{-}4)$$

and Young's modulus (*E*) was computed using:

$$E = 2\rho V_S^2(1 + v) \quad (3\text{-}5)$$

The storage modulus and Young's modulus results with respect to different curing times are shown in Figure 3.9a and Figure 3.9b, respectively; the error bars are the standard deviations. Both the storage and Young's moduli increased as epoxy cured. As curing progressed, more epoxy functional groups formed crosslinks that enhanced stiffness of the system, which increased the storage and Young's moduli. These results validated that the physical and mechanical properties of epoxy changed as it cured, which explains why ECT could measure changes in electrical permittivity over time.

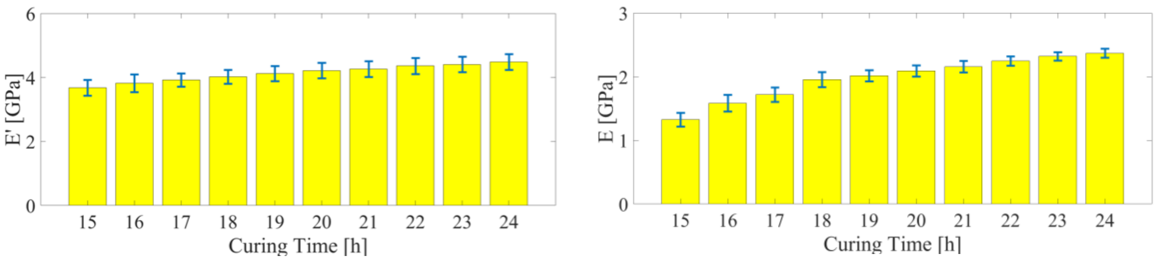

(a) (b)

Figure 3.9. The change in (a) the storage modulus and (b) the Young's modulus with respect to different curing times (*i.e.*, 15 to 24 h) are shown. Standard deviations of measured mechanical properties are also shown (based on three specimens tested).

3.5. Summary

In this chapter, a noncontact, noninvasive, imaging technique was proposed for monitoring pristine epoxy curing. First, quick-curing epoxy was used to validate ECT as a tool for capturing the electrical permittivity changes as epoxy cured in a relatively short time. Upon validating ECT and second, aerospace-grade epoxy was employed for the remainder of the tests and was subjected to 24-h room temperature curing monitoring experiments. The permittivity distributions were reconstructed using ECT at different curing times, and electrical permittivity changes were successfully monitored by ECT. Then, ultrasonic mechanical property tests were performed on the same material to measure changes in the storage and Young's moduli during curing. The ultrasonic characterization results showed that epoxy exhibited increases in its mechanical properties as curing progress, which further validated the ECT monitoring results. Last, ECT was also employed to simultaneously differentiate epoxy specimens at different curing stages placed in the sensing region together. The results demonstrated that ECT can be a viable technique to better understand the curing of pristine epoxy resins *in situ.*

Chapter 4. Carbon Nanotube-infused Epoxy Curing Monitoring

4.1. Introduction

The previous chapter discussed about applying ECT for monitoring curing of pristine epoxy. Besides using pristine epoxy resin as the matrix for FRP composites, multifunctional FRP composites that incorporate a suite of functionalities in addition to their load-carrying capability are receiving significant attention. One approach to realize multifunctional FRP composites is by infusing nanomaterials in the epoxy matrix to enhance their mechanical properties and to enable sensing functionality. However, fabrication of nanomaterial-enhanced epoxies remains challenging, since additives can hinder curing and affect the mechanical properties of FRP. Therefore, the objective of this chapter is to employ electrical capacitance tomography for monitoring curing in nanocomposite epoxies, and this chapter focuses on carbon nanotube-based epoxies whose electrical properties are sensitive to strain.

In this chapter, first, high-speed shear mixing and tip sonication were employed for dispersing multi-walled carbon nanotubes in epoxy. Specimens were fabricated and subjected to load tests in order to confirm their strain-sensitive electromechanical properties. Second, ECT was used to monitor nanocomposite epoxy curing, and the results confirmed that permittivity decreased with increasing curing time. Third, these results were then validated by ultrasonic testing, which estimated the elastic modulus of epoxy specimens subjected to different curing times. Last, a comparison experiment with pristine epoxy was performed. The results indicated that ECT was capable of identifying the difference between pristine and MWCNT-infused epoxy.

4.2. Experimental details

4.2.1. Specimens preparation

In this chapter, then same aerospace-grade EPON Resin 825 and Epikure Curing Agent 3046 but infused with MWCNTs (Nanointegris Technologies Inc.) were used to prepare specimens for electromechanical, ECT curing monitoring, and ultrasonic wave tests. First, all the specimens were prepared by measuring the required amounts of epoxy resin and curing agent using a 2:1 by mass ratio. Second, the epoxy resin was added to MWCNTs to obtain a 0.75 *wt.*% of MWCNTs, which was then subjected to high-speed shear-mixing for 5 min at 3,500 rpm. Further dispersion was performed by subjecting the MWCNT-resin mixture to ultrasonic probe sonication at 100 W amplitude for 3 min (*i.e.,* based on a run cycle of 2-s pulse-on and 5-s pulse-off). This procedure of shear-mixing and probe sonication was repeated for four more times to prevent overheating and to more effectively disperse large MWCNT agglomerations. Similarly, the curing agent was also mixed with MWCNTs to obtain a concentration of 0.75 *wt.*%, followed by high-speed shear mixing for 10 min at 3,500 rpm. Last, the MWCNT-resin and MWCNT-curing agent were combined and subjected to high-speed shear mixing for 10 min at 3,500 rpm to form the epoxy mixture.

Using the same MWCNT-infused epoxy, three different sets of specimens were casted for experiments conducted in this chapter. First, the electromechanical or strain sensing test specimens were cast in 50×10×1 mm^3 polydimethylsiloxane (PDMS) rectangular molds with copper tape electrodes pre-positioned 20 mm apart from each other. The copper tape electrodes were necessary for measuring their electrical response when strained. Second, ECT curing monitoring test specimens were casted in 20 mL glass vials. Last, MWCNT-infused epoxies were also casted in 20 cm-long plastic tubes for ultrasonic tests that were performed to characterize their mechanical properties during different stages of curing. All specimens were cured in a Yamato ADP-300C vacuum oven for 2 h at 40 ºC.

4.2.2. Electromechanical testing

Strain sensing tests of 50×10×1 mm^3 MWCNT-infused epoxy strips were conducted by subjecting each specimen to three cycles of uniaxial tensile cyclic loading while measuring their change in electrical properties. The test setup is shown in Figure 4.1a, where a Test Resources 150R load frame was employed to strain the specimen. The specimen's electrical resistance was measured using a Keysight 34401A digital multimeter (DMM), and the data was collected and recorded using the Keysight BenchVue data logging software. The gage length between the load frame's two grips was 40 mm. This setup ensured that both electrodes were in between the two grips to prevent straining of the electrodes and inflicting unwanted noise to the sensor measurements. All tests were performed in displacement-controlled mode, where the applied strain rate was 0.5%/min, and the peak strain was 0.5% or, equivalently, 0.2 mm of total elongation.

4.2.3. ECT curing monitoring test

ECT was employed for monitoring curing of MWCNT-infused epoxy specimens, which was similar to the monitoring test presented in chapter 3. First, upon pouring the MWCNT-infused epoxy into the 20 mL glass vial, the specimen was placed in the center of the ECT sensing area for measurements (Figure 4.1b). Second, the specimen was removed and placed in the vacuum oven (maintained at 40 ºC) to cure for 10 min. The specimen was then removed and then subjected to ECT testing again. This procedure was

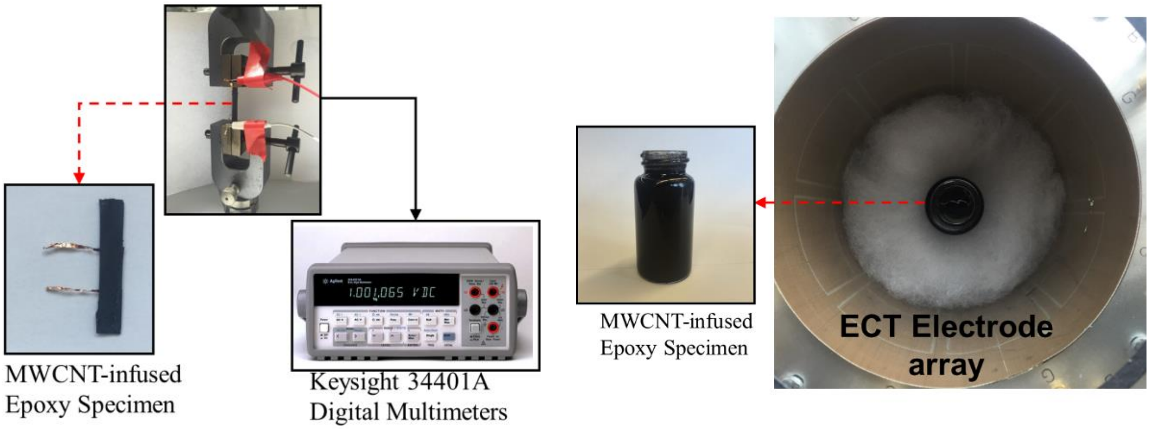

(a) (b)

Figure 4.1. (a) The schematic illustrates the test setup for conducting strain sensing test of MWCNT-infused epoxy specimens, and (b) MWCNT-infused epoxy specimens were individually placed inside the electrode array for ECT testing.

repeated such that ECT tests were performed every 10 min for a total curing time of 120 min. In total, five specimens were cured and tested following this procedure.

4.2.4. Characterization of mechanical properties

In order to further validate the ECT curing monitoring test results, ultrasonic wave propagation tests were also performed on MWCNT-infused epoxy specimens to characterize how their elastic properties changed during the curing process. In this chapter, shear waves were employed, and the time-of-flight of the wave propagating through the specimens was measured for calculating the specimen’s Young’s modulus. However, since shear waves can only propagate in solid-like media (*i.e.*, a glassy-rubber state for epoxy-based materials), the test specimens (casted in 20 mL plastic tubes) were first cured for 60 min at 40 ºC before being subjected to the first ultrasonic test. Similar to the ultrasonic wave test in chapter 3, characterization of mechanical properties was performed by coupling two PZT shear wave transducers to opposite ends of the MWCNT-infused epoxy specimen as shown in Figure 4.2. An Agilent 33250A function generator was employed to excite one of the PZT transducers with a 1 MHz pulse waveform, while the response signal was captured by the other PZT transducer on the opposite end, which is connected to a Keysight DSOX3024T oscilloscope that recorded and displayed the corresponding voltage response (Figure 4.2). Upon testing, the specimen was placed back in the vacuum oven to cure, and ultrasonic tests were conducted every 20 min until the specimen completely cured after 120 min of total curing time. Three different specimens were tested.

4.2.5. Curing comparison tests

As mentioned earlier, another set of ECT tests were performed on pristine and MWCNT-infused epoxy specimens for comparing the curing process. A new set of specimens were prepared using the same aerospace grade epoxy resin (*i.e.*, EPON Resin 825 and Epikure Curing Agent 3046). For pristine epoxy, the resin and curing agent were added together and subjected to high-speed shear mixing operated at 2,000 rpm for 10 min. On the other hand, MWCNTs were added to the resin to achieve a concentration of 0.5 *wt*.% for the other sample set. The MWCNT-resin mixture was subjected to high-speed shear mixing at 3,500 rpm for 40 min to disperse the nanotubes. Then, curing agent was added, and the shear mixer was again employed to blend the final mixture containing MWCNTs, resin, and curing agent. Both pristine and MWCNT-infused epoxy specimens were casted in 20 mL glass vials and subjected to ambient room temperature curing.

Curing monitoring tests were performed by first curing the epoxy mixtures for 13 h in room temperature. Thereafter, each specimen was placed in the center of the ECT electrode array for boundary capacitance interrogation and data acquisition, which is the same as that shown in Figure 4.1b. While each specimen continued to cure, ECT tests were conducted every 2 h until a maximum curing time of 23 h. The capacitance data

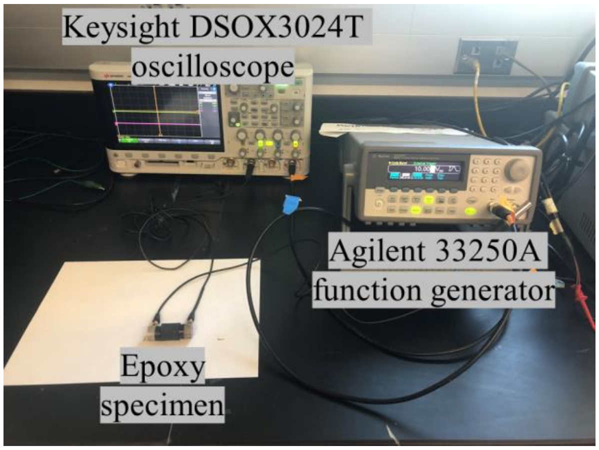

Figure 4.2. The experimental setup of the ultrasonic wave test for estimating the Young's modulus of MWCNT-infused epoxy specimens is shown.

corresponding to each curing time was acquired and used for spatial permittivity reconstruction. Instead of using the absolute reconstructed permittivity distribution, a baseline ECT test was also performed with the sensing region being empty (*i.e.*, filled with only air), and relative changes with respect to this baseline was obtained.

4.3. Results and discussion

4.3.1. Strain sensing response

The main objective of this chapter was to investigate the suitability of ECT for monitoring curing features in MWCNT-infused epoxies, especially since they are seeing more widespread use as a smart matrix material for FRP composites. As a result, many different nanocomposite- and MWCNT-based epoxies whose electrical properties are sensitive to strain were developed and reported. This work does not aim to propose a novel or better strain-sensitive nanocomposite epoxy. Instead, an MWCNT-infused epoxy formulation was developed and used for the purposes of demonstrating curing monitoring.

Nevertheless, to demonstrate that the MWCNT-infused epoxy specimens employed in this work could provide multifunctional properties for FRP composites, they were subjected to strain sensing characterization tests as detailed earlier. Figure 4.3a shows the normalized change in resistance (R_n) of a representative MWCNT-infused epoxy specimen plotted with respect to time when a three-tensile-cycle strain pattern to a peak strain of 0.5% was applied. R_n is:

$$R_n = \frac{(R - R_0)}{R_0} \tag{4-1}$$

where R is the resistance measured at any instant of time, and R_0 is the specimen's unstrained or nominal resistance. It should be mentioned that R_0 of the specimens was ~ 11.27±0.33 MΩ. Overall, it can be seen from Figure 4.3a that its R_n time history response correlates well with the applied strain pattern, thus validating its strain sensing behavior.

It can be hypothesized that the conductivity or resistivity of the MWCNT-infused epoxy was derived from the embedded MWCNTs forming conductive paths within the epoxy matrix. For the specimens prepared in this experiment, the concentration of MWCNTs was well past the percolation threshold. When strained, the intrinsic piezoresistivity of MWCNTs and the tunneling effect between neighboring MWCNTs was assumed to be the dominant factors that contributed to the strain-sensitive behavior observed [61]. However, some minor variations between the R_n time history and applied strain pattern were observed, where these differences could be due to noise, minor specimen slippage after each loading cycle, and/or its inherent viscoelastic properties.

To further characterize the MWCNT-infused epoxy specimens' strain sensing performance, one can plot R_n with respect to the corresponding applied strains, as is shown in Figure 4.3b. The result is approximately linear, and a linear least-squares regression line was fitted to the data. The slope of the best-fit line is:

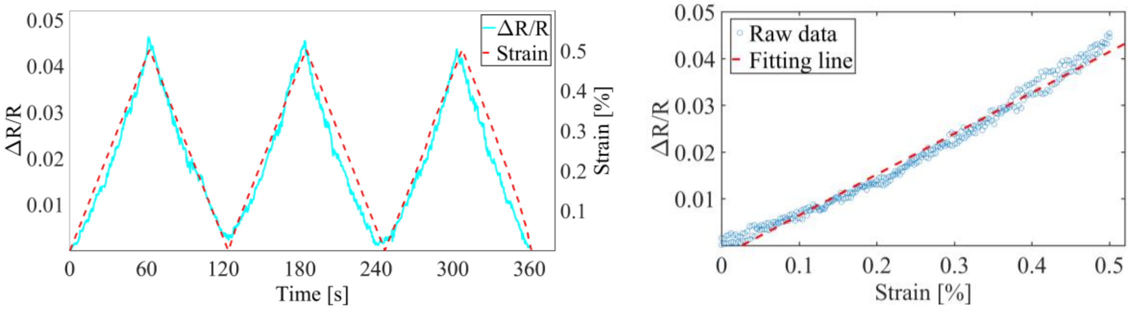

(a) (b)

Figure 4.3. (a) The normalized change in resistance time history of a specimen subjected to three cycles of tensile loading to 0.5% peak strain is shown. (b) The normalized change in resistance data plotted as a function of applied strains were fitted with a linear regression line.

$$S = \frac{R_n}{\varepsilon} \tag{4-2}$$

which is equivalent to the nanocomposite epoxy's strain sensitivity (*S*) or gage factor, and ε in equation (4-2) is the strain applied corresponding to R_n. The average strain sensitivity for all the specimens tested was ~ 9.84±0.84, where the error corresponds to the standard deviation. The result shown in Figure 4.3b also indicated the repeatability of the specimens' strain sensing properties, where R_n response over different cycles remain similar while exhibiting minimal hysteresis. In short, the MWCNT-infused epoxies exhibited favorable strain sensing properties and make them a good candidate for the remainder of this work.

4.3.2. ECT curing monitoring

As previously stated, ECT measurements were performed on five MWCNT-infused epoxy specimens casted in 20 mL glass vials for curing monitoring. The specimen was placed at the center of the ECT electrode array and interrogated every 10 min from 10 to 120 min. The corresponding reconstructed relative permittivity distributions are shown in

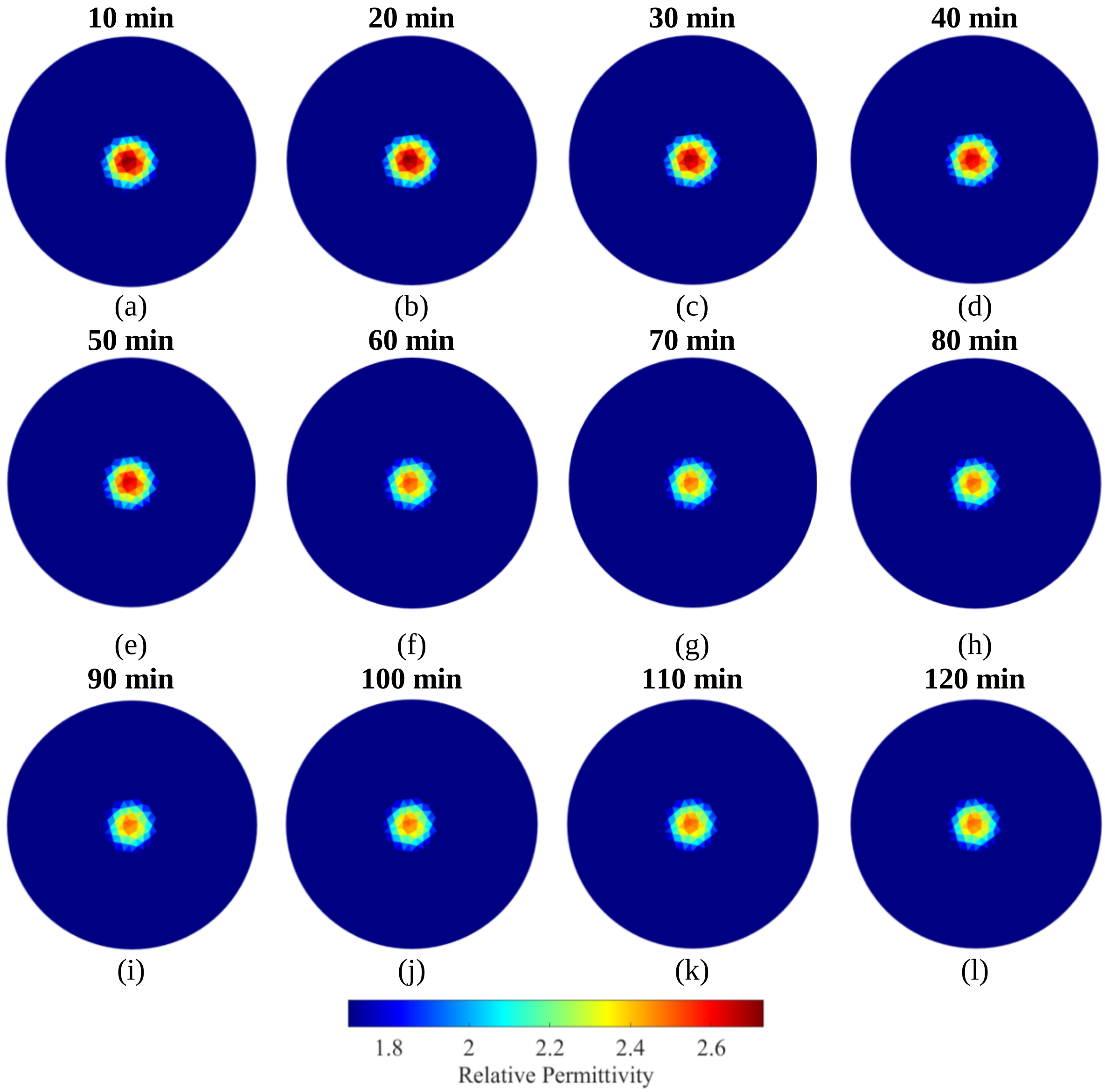

Figure 4.4. Relative permittivity distributions of epoxy specimens subjected to different curing times were reconstructed using ECT. ECT results of a representative MWCNT-infused epoxy specimen cured for (a) 10, (b) 20, (c) 30, (d) 40, (e) 50, (f) 60, (g) 70, (h) 80, (i) 90, (j) 100, (k) 110, and (l) 120 min are shown.

Figure 4.4. From these results, it can be observed that the epoxy specimens showed higher permittivity values at its initial stages (and when they were a viscous fluid). As curing reactions continued, the ECT results showed a reduction in permittivity. Similar to pristine epoxy discussed in chapter 3, as epoxy resin molecules reacted and formed crosslinks with

the curing agents, the specimen transferred from a viscous liquid to a solid state. It is hypothesized that the mobility of the ions inside the epoxy system decreases during phase change (*i.e.*, from liquid to solid), which causes a change in their dielectric characteristics. Besides accurately capturing the change in relative permittivity during curing, ECT was also able to precisely detect the location and size of the specimen in the sensing domain.

The average of the maximum relative permittivity values of five MWCNT-infused epoxy specimens, corresponding to each curing state, was calculated from reconstructed permittivity distributions and plotted with respect to curing time, as shown in Figure 4.5a. The error bars in Figure 4.5a correspond to the standard deviations of the five specimens tested. It can be seen from these results that the rate of change of relative permittivity was higher during the first 60 min, followed by gradually slowing down as curing time progressed. No significant change in permittivity was observed from 60 to 120 min. It should be noted that Figure 4.5a also shows that the relative permittivity of the MWCNT-infused epoxy specimens increased marginally as they cured from 10 to 20 min. This increase in relative permittivity could be due to temperature effects. As mentioned earlier, the epoxy specimens were cured at 40 ºC in a vacuum oven. During the initial stages of curing (*i.e.*, between 0 to 20 min), the specimen was still heating up. As the temperature of the MWCNT-based epoxy and resin mixture was increasing, it was becoming more liquid, thus exhibiting an increase in their permittivity. Once a steady-state temperature was reached, the effect of heating no longer became relevant, and electrical permittivity decreased due to the decrease in mobility of ions as the specimens solidified.

4.3.3. Young's modulus characterization

In order to further validate the aforementioned ECT curing monitoring results, ultrasonic tests were conducted on partially and completely cured epoxy specimens (*i.e.*, after 60 to 120 min of curing) to characterize their Young's modulus. As previous mentioned in chapter 3, to obtain the Young's modulus (*E*), the p- and s-wave velocities (*i.e.*, pressure and shear waves, respectively) were measured during the ultrasonic wave tests. In short, the p-wave is the weak longitudinal wave generated by the PZT transducer and corresponds to the first signal peak received (*i.e.*, due to its intrinsic faster group velocity); the second noticeable peak corresponds to the s-wave signal. The time-of-flight of the two waves were measured to calculate the p- and s-wave velocities (*i.e.*, V_P and V_S, respectively). After obtaining V_P and V_S, Poisson's ratio (v) of the specimen could be computed. The Young's modulus of the MWCNT-infused epoxy could then be estimated using Poisson's ratio (v) and V_S. The detailed equations are shown in section 3.4.2.

The results of the estimated Young's modulus values corresponding to different curing times are plotted in Figure 4.5b, and the error bars represent the standard deviations of the data. First, it should be mentioned that ultrasonic tests were not performed for specimens that were cured for less than 60 min, since the MWCNT-infused epoxy specimens were still in the viscous liquid state. Their shear strength remained too small to allow the propagation of shear waves through the medium, which prevented the detection of the second or s-wave peak. Second, for specimens cured for at least 60 min, they reached a glassy transition stage and possessed sufficient amounts of shear strength to ensure the propagation of shear waves for accurate estimation of Young's modulus [60]. This observation points to an important limitation of ultrasonic testing, since it cannot be

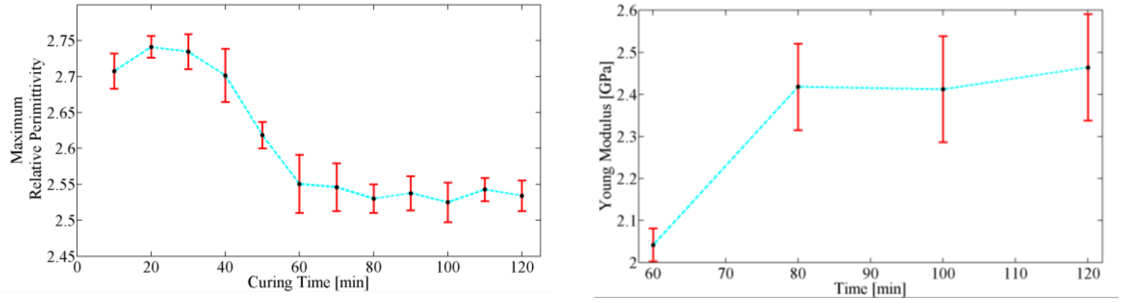

(a) (b)

Figure 4.5. (a) The ECT results were processed for five different MWCNT-infused epoxy specimens, and the average maximum relative permittivity of all specimens are plotted with respect to total curing time. The error bars correspond to the standard deviations. (b) The change in Young's modulus with respect to different curing times (*i.e.*, from 60 to 120 min) are shown. Standard deviations of measured Young's modulu are also shown (for four specimens tested).

employed to estimate the elastic properties of epoxy during early stages of curing; however, this technique can be used for curing monitoring once epoxy starts to solidify.

It can be seen from the results shown in Figure 4.5b that, from 60 to 80 min, *E* increased with increasing curing time. As curing reactions continued over time, more epoxy groups formed crosslinked structures that enhanced the stiffness of the epoxy system and increased the overall Young's modulus or stiffness of the material, which makes sense. After 80 min of curing, *E* remains relatively constant, which matches with what was observed from the ECT results (Figure 4.5a). Therefore, from the results shown in Figure 4.5, a conclusion is that permittivity change could be noninvasively monitored by ECT as an indicator of the degree of epoxy curing, especially for the entire curing process. It was found that permittivity of the MWCNT-infused epoxy specimens decreased over time as the epoxy cured and solidified.

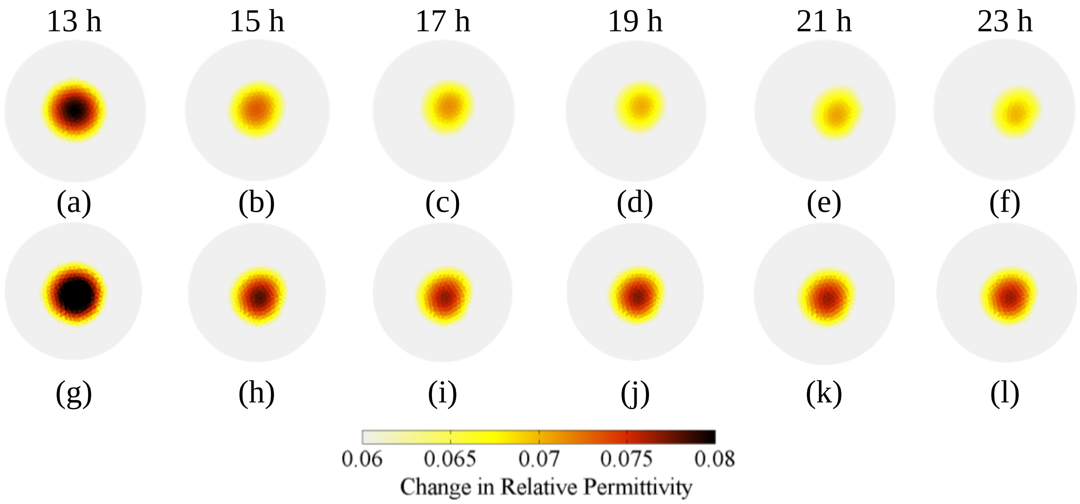

Figure 4.6. Changes in relative permittivity of epoxy specimens subjected to different curing intervals were mapped using ECT. ECT results of the pristine epoxy cured for (a) 13, (b) 15, (c) 17, (d) 19, (e) 21, and (f) 23 h are shown, and (g) to (l) show ECT results for an MWCNT-infused epoxy specimen subjected to the same curing schedule.

4.3.4. Comparison test

As was previously stated, ECT tests were performed on additional sets of pristine and MWCNT-infused epoxy specimens for comparing their curing process. First, Figure 4.6a to 4.6f show the reconstructed spatial permittivity maps of the entire sensing domain with a pristine epoxy specimen in the center as it was curing from 13 to 23 h in room temperature. These ECT results (Figure 4.6) show relative permittivity changes with respect to the baseline permittivity map of an empty sensing domain with just air. It can be seen from these results that ECT identified higher relative permittivity during initial stages of curing. As time progressed and curing continued, relative permittivity decreased as the specimens transitioned from a semi-viscous fluid state to the solid phase. Second, Figure 4.6g to 4.6l present the change in permittivity distributions for an MWCNT-infused epoxy specimen. Similar to the epoxy specimens discussed earlier, the permittivity changes also

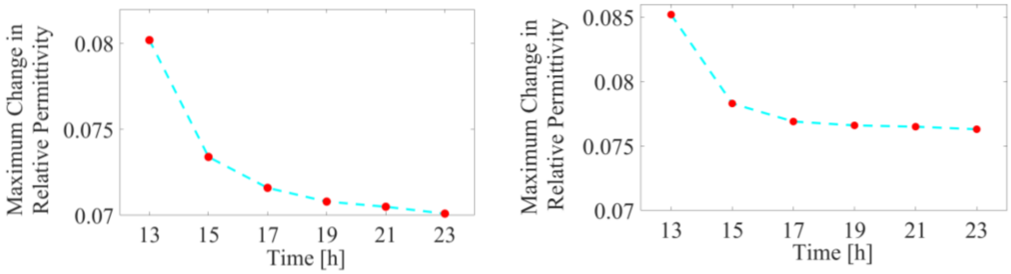

(a) (b)

Figure 4.7. The ECT results were processed, and the maximum change in relative permittivity of (a) pristine and (b) MWCNT-infused epoxy specimens are plotted with respect to total curing time.

decreased with respect to curing time. The results also clearly indicated that the relative permittivity values of MWCNT-infused epoxy are much greater than pristine epoxy throughout the monitored curing time.

To better quantify the relative permittivity changes, Figure 4.7 shows how the maximum change in relative permittivity, as identified by ECT and for both the pristine and MWCNT-infused specimens presented in Figure 4.6, varied as a function of curing time. First, the results suggested that the rate of electrical permittivity change decreased with respect to time, as was mentioned earlier in this chapter. Moreover, it can be seen from Figure 4.7 that the change in relative permittivity of the MWCNT-infused epoxy specimen reached a plateau in a shorter amount of time (Figure 4.7b) as compared to pristine epoxy (Figure 4.7a). Despite the fact that the change in permittivity of the MWCNT-infused epoxy specimen stabilized quicker, it was hypothesized that this did not signify faster curing. Qualitative observations during testing found that additives such as MWCNTs made it more difficult for epoxy to cure. Figure 4.7 shows that the magnitudes of the change in permittivity of both specimens were comparable at 13 h when ECT testing began, thereby indicating similar material properties at this stage. However, one can see by comparing Figures 4.7a and 4.7b that the change in relative permittivity plateaued to different magnitudes. The plateau for the MWCNT-infused case corresponded to a higher change in permittivity value, and its magnitude is comparable to when the pristine epoxy was cured for less than 15 h. This signified that MWCNTs limited the ability of the epoxy mixture to reach complete curing, and changes to the epoxy mixture design was needed to improve the curing process. A possible reason for this could be that the MWCNTs interacted with the free epoxide groups and prevented them from forming polymer chains as they normally would during pristine epoxy curing. The other possible explaination for MWCNT-infused epoxy specimens resulted in higher perimittivty could be that the MWCNTs changed the dielectric properties of the intrinsic material, since it possesses higher perimittivity than prsitine epoxy.

4.4. Summary

In this chapter, the objective was to validate that electrical capacitance tomography could be used as a noncontact and effective technique for monitoring curing in nanocomposite epoxy systems. First, an MWCNT-infused epoxy whose electrical properties were sensitive to strain was developed. High-speed shear mixing and probe sonication were employed for uniformly dispersing MWCNTs in both the epoxy resin and curing agent, before they were mixed and cured. Second, strain sensing characterization tests showed that the MWCNT-infused epoxy specimens showed high strain sensitivity (with a gage factor of ~ 9.8) with good linearity and repeatability. Third, using the ECT forward and inverse problems that was developed for this work and an ECT hardware system, the test setup was employed for experimentally monitoring the electrical permittivity of MWCNT-infused epoxy specimens as they cured to different time intervals.

The ECT results indicated that electrical permittivity decreased as curing time increased. Fourth, to validate these ECT results, the Young’s modulus of these epoxy specimens was also measured using ultrasonic tests. The evolution of Young’s modulus over time (*i.e.*, increasing from 60 to 80 min and then stabilizing thereafter) correlated well with how the electrical permittivity changed over time. Last, as compared to pristine epoxy specimens, MWCNT-infused epoxy resulted in higher permittivity values, which could be used to extinguish different specimens. Also, the different curing rates of the two sets of specimens was successfully monitored. Therefore, ECT can be used as a noncontact, nonintrusive imaging technique for *in situ* curing monitoring of nanocomposite epoxies.

Chapter 5. Subsurface Damage Detection

5.1. Introduction

As previous stated in chapter 1, besides monitoring the curing process of epoxy, it is also necessary to evaluate the durability and to ensure the integrity of FPR composites during while in service [62]. Therefore, the main objective of this chapter is to demonstrate ECT as a noncontact and portable technique for technicians to detect the presence of subsurface defects (or damage) in pristine and nanocomposite epoxies. The principle of ECT was explained in detail previously. In short, using an array of noncontact electrodes, an electric field is propagated to excite a structure, while capacitance measurements are obtained. The measurements are used to solve and reconstruct the permittivity distribution of the specimen interrogated. Manufacturing defects in the form of voids, which are air bubbles, also have different permittivity than cured epoxy. The hypothesis is that ECT can resolve the sizes and locations of these air voids in epoxy specimens.

In this chapter, helicopter rotor blade shape specimens were first casted by using quick-curing epoxy to validate the shape reconstruction and damage location identification ability of the ECT system. Second, disk-shaped MWCNT-infused epoxy specimens were subjected to damage by introducing a gradually enlarged hole to simulate different severities of damage, where the introduction of each new damage state was followed by ECT characterization. Finally, a similar test procedure was employed to test pristine and MWCNT-infused cylindrical epoxy specimens for validating damage detection.

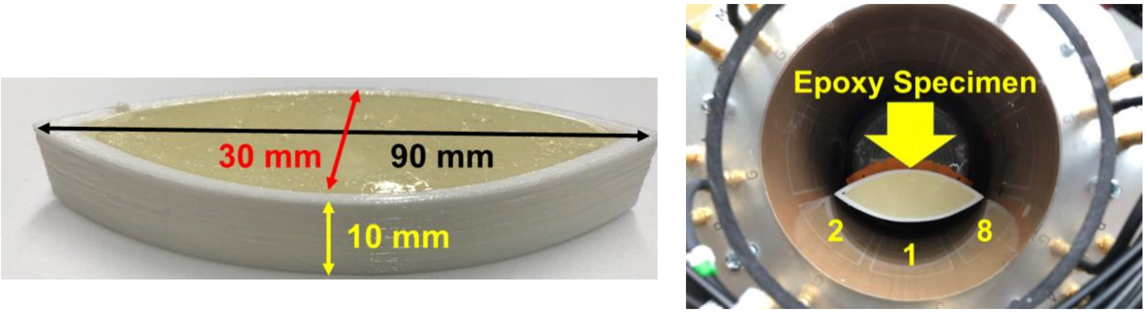

(a) (b)

Figure 5.1. (a) A helicopter rotor blade-shaped epoxy specimen was cast in a 3D-printed mold for ECT validation tests. (b) The specimen was placed in the ECT sensing domain for testing.

5.2. Experimental details

5.2.1. Helicopter rotor blade test

In order to validate that ECT can be used for subsurface damage detection in epoxy-based materials, a quick-curing epoxy (*i.e.*, 5 min of set time and 30 min of handling time) was used for the experiments. Two components of epoxy (*i.e.*, the resin and the hardener) were thoroughly mixed together by hand for 1 min. The specimens were based on a simplified helicopter rotor blade geometry. Here, a Ninjaflex mold (90 mm-length, 30 mm-width, and 10 mm-height), which is shown in Figure 5.1a, was printed using a Type A Series 1 Pro 3D printer. Upon printing, the quick-curing epoxy mix was poured into the mold and then cured in ambient room temperature. Prior to performing any validation tests , a baseline set of ECT measurements of the empty sensing domain (*i.e.*, with only air) was obtained. The first test then began by placing each pristine specimen in the ECT sensing domain as shown in Figure 5.1b (*i.e.*, near electrodes 1, 2, and 8) for ECT interrogation and data acquisition, where the goal was to assess the reconstructed shape of the specimen. The second set of tests focused on damaging the epoxy specimens by drilling a 4.7 mm-diameter hole at a different location on each specimen. In total, three damage locations were chosen as shown in Figure 5.2. Once damage was introduced, the specimen was placed back into approximately the same location in the sensing domain, and ECT measurements were acquired. Permittivity distributions were reconstructed from these measured sets of boundary capacitance data, and the ECT results were compared with respect to their corresponding undamaged cases.

5.2.2. Disk-shaped MWCNT-infused epoxy specimen

For the disk-shaped specimen, EPON Resin 825 and Epikure Curing Agent 3046 were used to prepare specimens for subsurface damage detection. The MWCNTs used here, which were the same as those in chapter 4, were manufactured by Nanointegris Technologies, Inc. To prepare the specimens, epoxy resin and curing agent were measured and mixed using a 2:1 mass ratio, as was previously described. Here, 0.75 *wt.*% of MWCNTs were dispersed into the epoxy resin by means of high-speed shear mixing (at 3,500 rpm for 40 min), followed by adding MWCNTs to curing agent and then shear-mixed for 10 min at 3,500 rpm. Then, MWCNT-infused epoxy resin and curing agent were combined and subjected to shear mixing for 10 min at 3,500 rpm. The specimen was cast in a large petri dish that was 86 mm in diameter and 9 mm in height, and then it was placed in Yamato ADP-300C vacuum oven for 2 h at 40 ºC for accelerated curing.

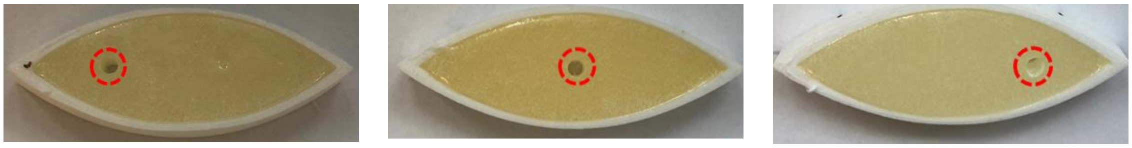
(a) (b) (c)

Figure 5.2. Epoxy specimens were damaged at three different locations, which corresponded to the (a) left, (b) center, and (c) right portion. A 4.70 mm-diameter masonry drill bit was used for introducing damage.

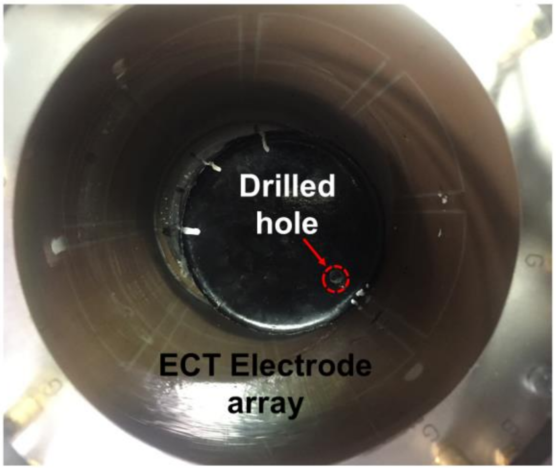

Figure 5.3. The disk-shaped MWCNT-infused epoxy specimen was placed in the ECT electrode array for interrogation and data acquisition. A drilled-hole damage was introduced near the boundary of the specimen, which was close to electrodes 7 and 8.

After completely curing the specimen, ECT was employed as a noncontact method for detecting subsurface damage. First, the test began by placing the undamaged specimen in the ECT sensing domain. The permittivity distribution of the undamaged specimen was reconstructed from the corresponding measured set of boundary capacitance responses and was used as the undamaged baseline relative to other damage states. Second, a 2.70 mm-diameter hole was drilled near the boundary of the specimen as a representative subsurface damage feature akin to a void. As shown in Figure 5.3, the location of the drilled hole is close to electrodes 7 and 8. Third, the damaged specimen was placed back in the ECT measurement system and at the same location (when recording the baseline) as shown in Figure 5.3. Then, drill bits of larger diameters were used for enlarging the already drilled hole, gradually, from 3.50 mm to 4.70 mm to 5.90 mm. After each drilling, the specimen was interrogated to obtain the corresponding capacitance response, which were then used as inputs to the ECT inverse problem for reconstructing the specimen's electrical permittivity distributions.

5.2.3. Cylindrical epoxy specimens

For cylindrical epoxy specimens, same aerospace-grade Hexion EPON Resin 825 and Epikure Curing Agent 3046 were used to fabricate epoxy specimens for subsurface defect detection validation tests. Two epoxy sample sets were casted, which are ones with pristine epoxy and another similar set but infused with MWCNTs. To prepare both sets of epoxy specimens, appropriate amounts of resin and curing agent were measured to achieve a 2:1 ratio (by mass). The detailed fabrication procedure for preparing these specimens has been described in section 4.2.5. It should be mentioned that specimens were casted in 40 mL cylindrical plastic containers, and both epoxy specimens were cured in ambient room temperature.

Cylindrical epoxy specimens (*i.e.*, 40 mm in diameter and 35 mm in height) that were cured for 72 h in ambient room temperature were subjected to ECT subsurface defect/damage detection tests. Similar to the previous damage detection tests, the test began by placing each undamaged specimen near electrode 8 of the ECT electrode array for interrogation and data acquisition. This capacitance dataset was used for reconstructing the permittivity distribution of the undamaged baseline case. Then, a hole was drilled in the center of each test specimen using a power drill. The diameter of the first drilled hole was 3.60 mm. Upon drilling, the specimen was placed back in the same location in the ECT sensing region for testing. The test continued by drilling a larger diameter hole in the same location, where hole diameter was gradually increased from 3.60 mm to 5.90 mm. ECT measurements were obtained after each drilling, which were then used for spatial permittivity reconstruction.

5.3. Results and discussion

5.3.1. Helicopter rotor blade test results

The damage detection validation tests focused on quick-curing epoxy specimens casted in 3D-printed helicopter rotor blade-shaped molds. A representative ECT result of the pristine specimen is shown in Figure 5.4. In Figure 5.4, the change in relative permittivity is shown, where the relative permittivity distribution of the baseline of air (*i.e.*, empty sensing domain) was subtracted from the test result. It can be observed from Figure 5.4 that the shape, size, and location of the helicopter rotor blade-shaped epoxy specimen was successfully detected by ECT. One can clearly observe the elliptical shape of the specimen. However, it should be mentioned that the sharp corners or edges of the specimen could not be fully reconstructed and appear rounded in the ECT result shown in Figure 5.4. This is expected due to smoothing effects induced by regularization. Nevertheless, the results successfully identified the general shape, location, and size of the system tested.

For further validation, damage was introduced to the pristine epoxy specimens by drilling a hole at a different location in each specimen, and the specimen was placed back (at the same location) in the ECT system. Representative ECT results for each of three damage locations are presented in Figure 5.5. In Figure 5.5, the change in relative permittivity distributions are plotted, and these were obtained by subtracting the permittivity map of the damaged specimen with its corresponding undamaged one to only reveal the change in permittivity due to each drilled hole. It can be clearly seen from Figure 5.5 that the three drilled holes at the left, center, and right portions of the specimens were

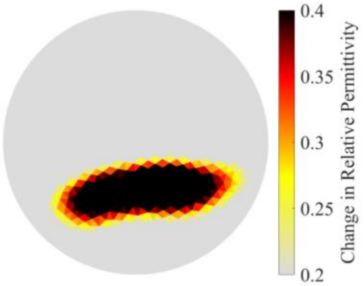

Figure 5.4. The shape and location of the helicopter rotor blade-shaped epoxy specimen was successfully captured using ECT.

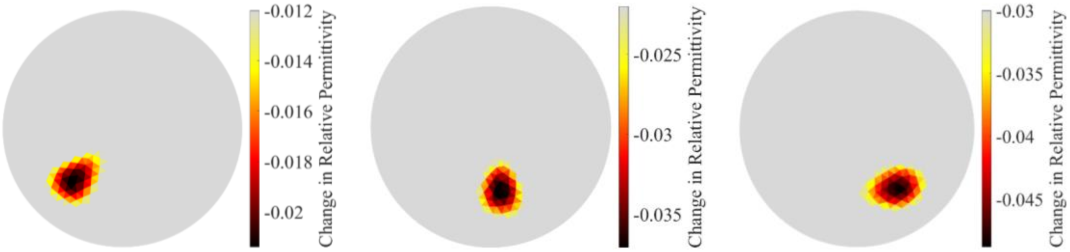

(a) (b) (c)

Figure 5.5. The ECT results corresponding to the damage at the (a) left, (b) center, and (c) right portion of different specimens are shown.

accurately identified by ECT. Therefore, these results validated that ECT can be used as a noncontact and noninvasive electrical imaging tool for detecting subsurface damage.

5.3.2. Disk-shaped MWCNT-infused epoxy specimen

A larger disk-shaped MWCNT-infused epoxy specimen was casted and used for ECT subsurface damage detection tests. First, an undamaged MWCNT-infused epoxy specimen was placed in the ECT electrode array, as shown in Figure 5.3, for acquiring the undamaged or baseline permittivity map. Damage was introduced by drilling larger and larger diameter holes at the same location of each specimen. The drilled-hole damage simulated a void in the epoxy-based system, with the intensity of damage increasing gradually as larger diameter holes were introduced. Upon drilling each hole, the specimen was placed back in the ECT sensing domain, at approximately the same location,

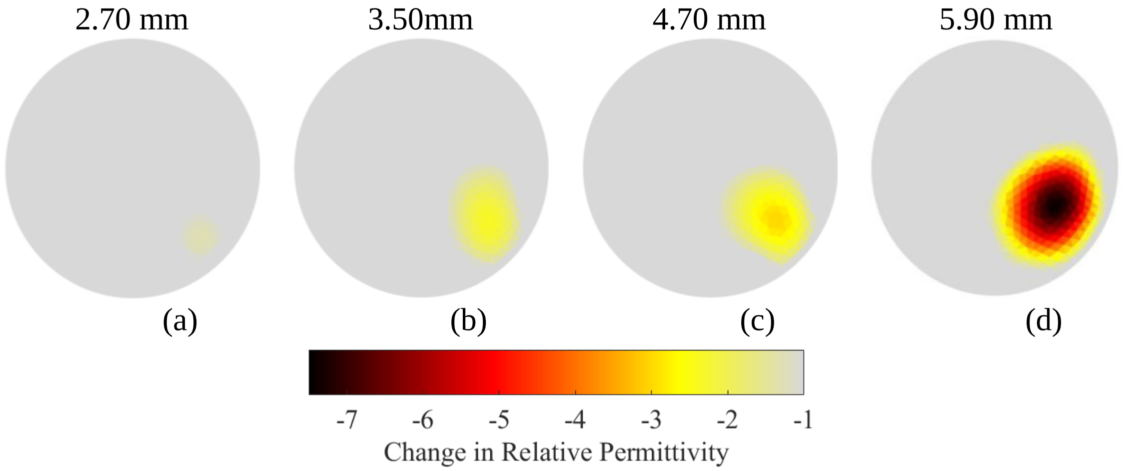

Figure 5.6. Subsurface damage was introduced in MWCNT-infused epoxy specimen by drilling holes of different sizes at the same location. The ECT results corresponding to a drilled hole of diameter (a) 2.70, (b) 3.50, (c) 4.70, and (c) 5.90 mm are shown (*i.e.*, with respect to a baseline of its undamaged state).

interrogated, and the corresponding electrical permittivity distribution was reconstructed from the measured sets of boundary capacitance responses.

As showing in Figure 5.6, ECT was able to accurately identify the corresponding location and severity of the drilled-hole damage. It should be noted that the results in Figure 5.6 show the change in relative permittivity distribution with respect to the undamaged baseline; thus, only the damage features are shown in the ECT results. A decrease in permittivity was observed near the vicinity of the introduced damage since more epoxy was removed as the diameter of the hole became larger. This can be explained by the fact that the drilled hole was filled with air, which has a lower permittivity than epoxy. Despite the ability of ECT to detect the location and severity of damage, it should be mentioned that the estimated size of damage is larger than the actual damage. This was most likely due to the inherent resolution of the ECT system employed, which is mainly governed by the number of independent measurements along with the regularization scheme adopted for solving the ECT inverse problem. Future studies will consider the fabrication and use of an ECT system with significantly more number of boundary electrodes, and sensing resolution and accuracy will be quantified. In the meantime, the results presented in this section successfully validated ECT for damage detection.

5.3.3. Cylindrical epoxy specimens

Another set of damage detection tests was performed on cylindrical epoxy specimens to further validate that ECT could be used as a nondestructive and noncontact tool for detecting subsurface defects or damage in materials. First, a pristine epoxy specimen was placed near electrode 8 as illustrated in Figure 5.7a, and a baseline ECT measurement of the undamaged specimen was obtained. Second, a 3.60 mm-diameter drill bit was employed to drill a hole in the center of the specimen. The drilled specimen was then placed back at the same location in the sensing region, followed by ECT testing. This procedure was repeated but by introducing a larger size of damage by drilling a larger diameter hole. For each case, the permittivity distribution was reconstructed using the

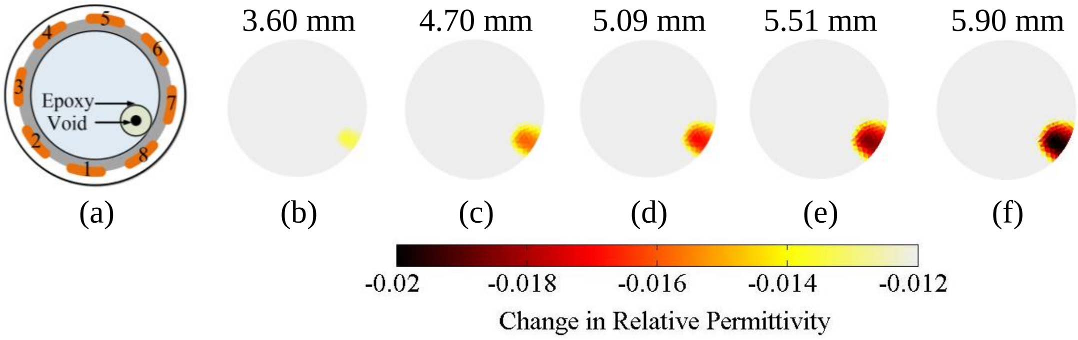

Figure 5.7. (a) Cured pristine epoxy specimen was subjected to subsurface damage ECT tests. The spatial permittivity maps corresponding to drilled holes of diameter (b) 3.60, (c) 4.70, (d) 5.09, (e) 5.51, and (f) 5.90 mm are shown (*i.e.*, with respect to a baseline of its undamaged state).

boundary capacitance measurements as inputs to the ECT inverse problem. Figures 5.7b to 5.7f show the ECT spatial permittivity maps corresponding to different sizes of damage introduced to the same specimen (*i.e.*, taken with respect to the undamaged baseline). Overall, Figure 5.7 confirmed that ECT was able to detect the location and sizes of induced damage. It was found that the size of the region of change in permittivity increased in tandem with increasing damage severity, which is consistent with the results discussed in previous section.

The same types of damage were introduced to MWCNT-infused epoxies. It can be seen from Figure 5.8 that the location and severity of damage (*i.e.*, to simulate manufacturing defects or voids) were accurately captured by ECT. Similar to section 5.3.2, the estimated size of defect is slightly larger than the actual drilled hole. Again, this was most likely due to the inherent resolution of the ECT system, which is governed by the number of independent measurements, along with the regularization scheme adopted.

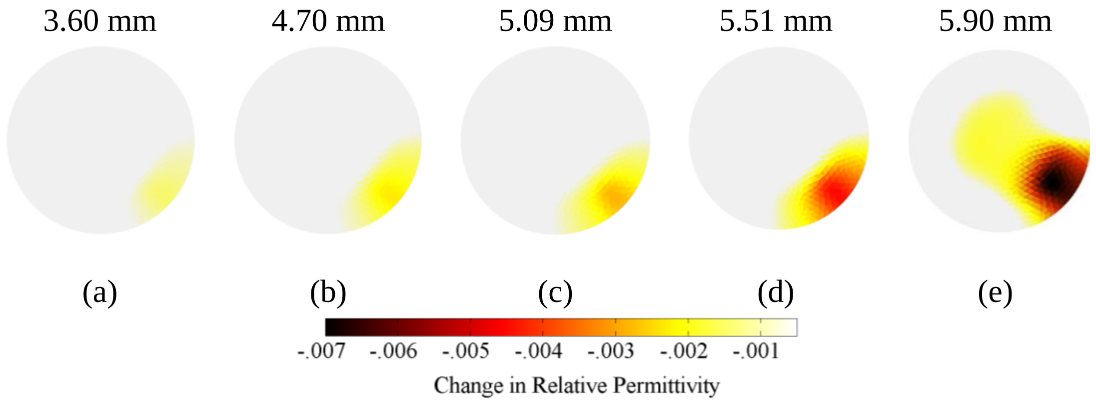

Figure 5.8. Subsurface damage was created in fully cured MWCNT-infused epoxy specimens. Damage was induced by drilling holes of different sizes, and the ECT results corresponding to drilled holes of diameter (b) 3.60, (c) 4.70, (d) 5.09, (e) 5.51, and (f) 5.90 mm are shown (*i.e.*, with respect to a baseline of its undamaged state).

Nevertheless, Figures 5.7 and 5.8 successfully validated the capability of ECT to detect subsurface damage in these epoxy-based cylindrical specimens.

5.4 Summary

In this chapter, first, the ability of ECT shape reconstruction was demonstrated. Quick-curing epoxy was cast in a simplified helicopter rotor blade mold, and ECT tests were performed to reconstruct the shape of the specimen. The results indicated that the ECT technique was capable of identifying the specimen location and its shape. Second, three holes were drilled at three different locations of the rotor blade specimens to simulate damage, and ECT was employed to detect these damage states. After subtracting the permittivity distribution of the undamaged specimens, the three drilled holes were accurately identified at their corresponding locations. Third, ECT was also employed to detect subsurface defects and voids in the disk-shaped MWCNT-infused epoxy specimens. A hole was initially drilled and then gradually enlarged to simulate the growth of subsurface damage during the service life of the structure. A similar test procedure was performed on cylindrical epoxy specimens using pristine and MWCNT-infused epoxies. All the results demonstrated that ECT was able to detect the location and severity of the introduced damage by showing a corresponding decrement in the permittivity distribution near the vicinity of the introduced damage.

Chapter 6. Conclusions

6.1. Summary

The main objective of this thesis was to validate electrical capacitance tomography as a noncontact and noninvasive technique for monitoring curing and for detecting subsurface damage in pristine and nanocomposite epoxy systems. In chapter 2, the theoretical formulation of ECT, including the forward and inverse problems, was presented. In general, ECT is a soft-field imaging technique that could reconstruct the electrical permittivity distribution of a sensing domain using sets of boundary capacitance measurements. The forward problem seeks to estimate the mutual capacitance of excitation-sensing electrode pairs given a known permittivity distribution and appropriate boundary conditions. Experimentally, the ECT inverse problem needs to be solved. The measurement strategy entails exciting an electrode with an alternating current, while other electrodes are grounded. The capacitance between excitation-sensing electrode pairs could then be measured using a high-speed capacitance data acquisition unit. The objective of the inverse problem is to minimize the error norm between the measured boundary capacitance and forward problem estimates of boundary capacitance using a Gauss-Newton iterative algorithm.

Chapter 3 focused on demonstrating ECT for monitoring curing of pristine epoxy. The change in dielectric property (*i.e.*, electrical permittivity) of epoxy specimens subjected to different curing times was captured by ECT, and these results were further validated using ultrasonic tests that revealed the specimens' mechanical properties at different stages of curing. In addition, ECT could resolve where these permittivity changes occurred in the sensing domain and could differentiate between different degrees of curing.

Chapter 4 proceeded to demonstrate that ECT could be extended to monitor curing of strain-sensitive MWCNT-infused epoxies. In order to uniformly disperse MWCNTs in epoxy resin and curing agent, high-speed shear mixing and probe sonication techniques were employed. The strain sensitivity of the MWCNT-infused epoxy specimens was characterized to be ~ 9.8. The MWCNT-infused epoxy specimens were cured at 40 ºC for 2 h, and ECT was utilized to monitor the curing process of these nanocomposite epoxies. The ECT results indicated that their electrical permittivity decreased as curing time increases. The Young's modulus of these MWCNT-infused epoxy specimens was also characterized using ultrasonic wave tests to validate the ECT results. It was found that the change in mechanical properties of epoxy as they cured followed a similar trend as how electrical permittivity changed during curing. A comparison test between pristine and MWCNT-infused epoxy was performed, and the results indicated that ECT can successfully identify the permittivity difference between two specimens as they cured.

Finally, the aim of chapter 5 was to validate ECT for detecting subsurface defects and damage. The chapter started with ECT shape reconstruction validation tests using quick-curing epoxy that was casted to form a helicopter rotor blade-like structure. Then, subsurface damaged detection tests were performed on three different shapes of specimens (*i.e.*, helicopter rotor blade, disk, and cylinder). Damage was introduced by drilling holes at different locations and enlarged to different sizes for simulating damage propagation. The results indicated that ECT could accurately locate damage and detect damage severity.

6.2. Future work

In the future, improving the sensing resolution of the ECT system is one of the most difficult but also most necessary tasks that need to be performed. This can be achieved by implementing an ECT system with higher number of boundary electrodes or by improving the regularization scheme used in the inverse problem. Furthermore, the current ECT hardware is restricted by the size (or diameter) of the sensing domain. Therefore, different ECT electrode arrangements could be developed so that ECT can be applied to a broader range of specimens and applications.

From a curing monitoring perspective, ECT can be used to monitor different cross-sections of the same epoxy specimen curing, and the results can be used to generate a 3D electrical permittivity representation of the entire structure. Such a scanning ECT system can reveal non-uniform curing in complex 3D structural parts. In addition, future research will also explore if this MWCNT-infused epoxy can be used as a strain-sensitive matrix for manufacturing FRP structures and components. ECT will be applied for *in situ* curing monitoring and subsurface damage detection of more realistic FRP components to demonstrate their applicability for monitoring various aerospace, civil, marine, and mechanical structures.

6.3. Reproduction of published content

Parts of Chapter 2 and the entirety of Chapters 3, 4, and 5 are reprints of the material as it appears in Noncontact Epoxy Curing Monitoring and Subsurface Damage Detection, Proceedings of the 11th international workshop on structural health monitoring, 2017, Gupta S, Fan G, Loh KJ, and Noninvasive Monitoring of Epoxy Curing. IEEE Sensors Letters, 2017, 1(5), Gupta S, Fan G, Loh KJ. The thesis author was the primary investigator and co-author on these two papers. In addition, some of the work that appears in this thesis was submitted for consideration for publication in Curing and Subsurface Damage Monitoring of Epoxy-based Composites, Structural Health Monitoring, 2017, Fan G, Gupta S, Loh KJ. The thesis author was the primary investigator and first author of this paper.

References

[1] Reddy C, Sagar V. Two-Dimensional Theoretical Modeling of Anisotropic Wear in Carbon/Epoxy FRP Composites: Comparison with Experimental Data. International Journal of Theoretical and Applied Mechanics. 2011;6.

[2] Gupta S, Fan G, Loh KJ. Noncontact Epoxy Curing Monitoring and Subsurface Damage Detection 11th international workshop on structural health monitoring; Stanford, CA: Destech Publications, Inc; 2017.

[3] Kahandawa GC, Epaarachchi J, Wang H, Lau KT. Use of FBG Sensors for SHM in Aerospace Structures. Photonic Sensors. 2012;2(3).

[4] Wu Z, Wang X, Zhao X, Noori M. State-of-the-art review of FRP composites for major construction with high performance and longevity. International Journal of Sustainable Materials and Structural Systems. 2014;1(3).

[5] Phil E, Soutis C. Polymer composites in the aerospace industry: Elsevier; 2014.

[6] Garg AC, Mai Y-W. Failure mechanisms in toughened epoxy resins—A review. Composites Science and Technology. 2006;31(3).

[7] Coope TS, Turkenburg DH, Fischer HR, Luterbacher R, van Bracht H, Bond IP. Novel Diels-Alder based self-healing epoxies for aerospace composites. Smart Materials and Structures. 2016;25(8).

[8] George P, Bhowmik S, Abraham M, Sriram P, Pitchan Mk, Ajeesh G. High-performance fire-resistant polymeric nanocomposite for aerospace applications. Proceedings of the Institution of Mechanical Engineers, Part L: Journal of Materials: Design and Applications. 2016.

[9] May C. Epoxy resins: chemistry and technology: Marcel Dekker; 1987.

[10] Nguyen H-V, Andreassen E, Kristiansen H, Johannessen R, Hoivik N, Aasmundtveit KE. Rheological characterization of a novel isotropic conductive adhesive – Epoxy filled with metal-coated polymer spheres. Materials & Design. 2013;46.

[11] Katariya MN, Jana AK, Parikh PA. Corrosion inhibition effectiveness of zeolite ZSM-5 coating on mild steel against various organic acids and its antimicrobial activity. Journal of Industrial and Engineering Chemistry. 2013;19(1).

[12] Kandare E, Kandola BK, Myler P. Evaluating the influence of varied fire-retardant surface coatings on post-heat flexural properties of glass/epoxy composites. Fire Safety Journal. 2013;58.

[13] Azeez AA, Rhee KY, Park SJ, Hui D. Epoxy clay nanocomposites – processing, properties and applications: A review. Composites Part B: Engineering. 2013;45(1).

[14] van Wachem PB, A. BL, Zeeman R, Dijkstra PJ, Feijen J, Hendriks M, Cahalan PT, van Luyn MJA. In Vivo Behavior of Epoxy-Crosslinked Porcine Heart Valve Cusps and Walls. Journal of Biomedical Materials Research Part A. 2000;53(1).

[15] Jin F-L, Ma C-J, Park S-J. Thermal and mechanical interfacial properties of epoxy composites based on functionalized carbon nanotubes. Materials Science and Engineering: A. 2011;528(29-30).

[16] Jin F-L, Park S-J. Thermal properties and toughness performance of hyperbranched-polyimide-modified epoxy resins. Journal of Polymer Science Part B: Polymer Physics. 2006;44(23).

[17] Xu H-J, Jin F-L, Park S-J. Synthesis of a Novel Phosphorus-containing Flame Retardant for Epoxy Resins. Bulletin of the Korean Chemical Society. 2009;30(11).

[18] Jin F-L, Li X, Park S-J. Synthesis and application of epoxy resins: A review. Journal of Industrial and Engineering Chemistry. 2015;29.

[19] Todoroki A, Omagari K, Shimamura Y, Kobayashi H. Matrix crack detection of CFRP using electrical resistance change with integrated surface probes. Composites Science and Technology. 2006;66(11-12).

[20] Schubel PJ, Crossley RJ, Boateng EKG, Hutchinson JR. Review of structural health and cure monitoring techniques for large wind turbine blades. Renewable Energy. 2013;51.

[21] Schroeder K, Ecke W, Apitz J, Lembke E, Lenschow G. A fibre Bragg grating sensor system monitors operational load in a wind turbine rotor blade. Measurement Science and Technology. 2006;17(5).

[22] Wernicke J, Shadden J, Kuhnt S, Byars R, Rhead P, Damaschke M. Field experience of fibre optical strain sensors for providing real time load information from wind turbine blades during operation. European Wind Energy Conference; London 2004.

[23] Balageas D, Fritzen CP, Guemes A. Structural Health Monitoring: Wiley-ISTE; 2006.

[24] Dutton AG. Thermoelastic stress measurement and acoustic emission monitoring in wind turbine blade testing. European Wind Energy Conference London 2004.

[25] Avdelidis NP, Almond DP, Ibarra-Castanedo C, Bendada A, Kenny S, Maldague X. Structural integrity assessment of materials by thermography. Damage in Composite Materials CDCM; Stuttgart, Germany 2006.

[26] Stanley P. Applications and potential of thermoelastic stress analysis. Journal of Materials Processing Technology. 1997;64(1-3).

[27] Haj-Ali R, Wei B-S, Johnson S, El-Hajjar R. Thermoelastic and infrared-thermography methods for surface strains in cracked orthotropic composite materials. Engineering Fracture Mechanics. 2008;75(1).

[28] Raghavan A, Cesnik CES. Review of Guided-wave Structural Health Monitoring. The Shock and Vibration Digest. 2007;39(2).

[29] Fahr A, Kandeil AY. Ultrasonic C-scan inspection of composite mateials. Engineering Journal of Qatar University. 1992;5.

[30] Ciang CC, Lee J-R, Bang H-J. Structural health monitoring for a wind turbine system: a review of damage detection methods. Measurement Science and Technology. 2008;19(12).

[31] Siringoringo DM, Fujino Y. Experimental study of laser Doppler vibrometer and ambient vibration for vibration-based damage detection. Engineering Structures. 2006;28(13).

[32] Pawar PM, Ganguli R. Helicopter rotor health monitoring- a review. Proceedings of the Institution of Mechanical Engineers, Part G: Journal of Aerospace Engineering. 2007;221(5).

[33] Hardis R, Jessop JLP, Peters FE, Kessler MR. Cure kinetics characterization and monitoring of an epoxy resin using DSC, Raman spectroscopy, and DEA. Composites Part A: Applied Science and Manufacturing. 2013;49.

[34] Lapique F, Redford K. Curing effects on viscosity and mechanical properties of a commercial epoxy resin adhesive. International journal of adhesion and adhesives. 2002;22(4).

[35] Shigue CY, dosSantos RGS, Baldan CA, Ruppert-Filho E. Monitoring the Epoxy Curing by the Dielectric Thermal Analysis Method. IEEE Transactions on Appiled Superconductivity. 2004;14(2).

[36] Tzounis L, Liebscher M, Tzounis A, Petinakis E, Paipetis AS, Mäder E, Stamm M. CNT-grafted glass fibers as a smart tool for epoxy cure monitoring, UV-sensing and thermal energy harvesting in model composites. RSC Adv. 2016;6(60).

[37] Gojny FH, Wichmann MHG, Fiedler B, Kinloch IA, Bauhofer W, Windle AH, Schulte K. Evaluation and identification of electrical and thermal conduction mechanisms in carbon nanotube/epoxy composites. Polymer. 2006;47(6).

[38] Shi X, Nguyen TA, Suo Z, Liu Y, Avci R. Effect of nanoparticles on the anticorrosion and mechanical properties of epoxy coating. Surface and Coatings Technology. 2009;204(3).

[39] Neitzert HC, Vertuccio L, Sorrentino A. Epoxy/MWCNT Composite as Temperature Sensor and Electrical Heating Element. IEEE Transactions on Nanotechnology. 2011;10(4).

[40] Lachman N, Daniel Wagner H. Correlation between interfacial molecular structure and mechanics in CNT/epoxy nano-composites. Composites Part A: Applied Science and Manufacturing. 2010;41(9).

[41] Hu N, Karube Y, Arai M, Watanabe T, Yan C, Li Y, Liu Y, Fukunaga H. Investigation on sensitivity of a polymer/carbon nanotube composite strain sensor. Carbon. 2010;48(3).

[42] Soleimani M. Image and shape reconstruction methods in magnetic induction and electrical impedance tomography: University of Manchester; 2005.

[43] Chaplin G, Pugsley T, Lee Lvd, Kantzas A, Winters C. The dynamic calibration of an electrical capacitance tomography sensor applied to the fluidized bed drying of pharmaceutical granule. Measurement Science and Technology. 2005;16(6).

[44] Huang SM, Plaskowsk AB, Xie CG, Beck MS. Tomographic imaging of two-component flow using capacitance sensors. Journal of Physics E: Scientific Instruments. 1989;22(3).

[45] Jaworski AJ, Dyakowski T. Application of electrical capacitance tomography for measurement of gas-solids flow characteristics in a pneumatic conveying system. Measurement Science and Technology. 2001;22(8).

[46] Yang WQ, Chondronasios A, Nattrass S, Nguyen VT, Betting M, Ismail I, McCann H. Adaptive calibration of a capacitance tomography system for imaging water droplet distribution. Flow Measurement and Instrumentation. 2004;15(5-6).

[47] Waterfall RC, He R, Wihite NB, Beck CM. Combustion imaging from electrical impedance measurements. Measurement Science and Technology. 1996;7(3).

[48] Dyakowski T, York T, Mikos M, Vlaev D, Mann R, Follows G, Boxman A, Wilson M. Imaging nylon polymerisation processes by applying electrical tomography. Chemical Engineering Journal. 2000;77(1).

[49] Al Hosani E, Zhang M, Soleimani M. A Limited Region Electrical Capacitance Tomography for Detection of Deposits in Pipelines. IEEE Sensors Journal. 2015;15(11).

[50] Gupta S, Loh KJ. Numerical simulations of railroad track damage characterization using non-contact tomography. 1st International Workshop on Structural Health Monitoring for Railway System; Qingdao, China: Destech Publications, Inc; 2016.

[51] Yin X, Hutchins DA. Non-destructive evaluation of composite materials using a capacitive imaging technique. Composites Part B: Engineering. 2012;43(3).

[52] Gupta S, Fan G, Loh KJ. Noninvasive Monitoring of Epoxy Curing. IEEE Sensors Letters. 2017;1(5).

[53] Soleimani M, Lionheart WRB. Nonlinear image reconstruction for electrical capacitance tomography using experimental data. Measurement Science and Technology. 2005;16(10).

[54] Gupta S, Loh KJ. Noncontact Electrical Permittivity Mapping and pH-Sensitive Films for Osseointegrated Prosthesis and Infection Monitoring. IEEE Trans Med Imaging. 2017;36(11).

[55] Bar-Cohen Y, Chatterjee A, West M. Sensors for cure monitoring of composite materials. Review of Progress in Quantitative Nondestructive Evaluation; La Jolla, CA: Springer; 1993.

[56] Barton JM. The application of differential scanning calorimetry (DSC) to the study of epoxy resin curing reactions. Epoxy Resins and Composites I Advances in Polymer Science. 1985;72.

[57] Wang FW, Lowry RE, Fanconi BM. Novel fluorescence method for cure monitoring of epoxy resins. Polymer. 1986;27(10).

[58] Lyon RE, Chike KE, Angle SM. In situ cure monitoring of epoxy resins using fiber-optic Raman spectroscopy. Applied Polymer Science. 1994;53(13).

[59] Maffezzoli A, Quarta E, Luprano VAM, Montagna G, Nicolais L. Cure monitoring of epoxy matrices for composites by ultrasonic wave propagation. Applied Polymer Science. 1999;73(10).

[60] Ghodhbani N, Maréchal P, Duflo H. Ultrasound monitoring of the cure kinetics of an epoxy resin: Identification, frequency and temperature dependence. Polymer Testing. 2016;56.

[61] Lee BM, Loh KJ. A 2D percolation-based model for characterizing the piezoresistivity of carbon nanotube-based films. Journal of materials science. 2015;50(7).

[62] Satori K, Ikeda Y, Kurosawa Y, Hongo A, Takeda N. Development of small-diameter optical fiber sensors for damage detection in composite laminates. SPIE's

7th Annual International Symposium on Smart Structures and Materials; Newport Beach, CA: International Society for Optics and Photonics.; 2000.